EUROPEAN RESPIRATORY *journal*

FLAGSHIP SCIENTIFIC JOURNAL OF ERS

Early View

Original research article

Pirfenidone exacerbates Th2-driven vasculopathy in a mouse model of SSc-ILD

Anna Birnhuber, Katharina Jandl, Valentina Biasin, Elisabeth Fließer, Francesco Valzano, Leigh M Marsh, Christina Krolczik, Andrea Olschewski, Jochen Wilhelm, Wolfgang Toller, Akos Heinemann, Horst Olschewski, Malgorzata Wygrecka, Grazyna Kwapiszewska

Please cite this article as: Birnhuber A, Jandl K, Biasin V, *et al*. Pirfenidone exacerbates Th2-driven vasculopathy in a mouse model of SSc-ILD. *Eur Respir J* 2022; in press (https://doi.org/10.1183/13993003.02347-2021).

Pirfenidone exacerbates Th2-driven vasculopathy in a mouse model of SSc-ILD

Birnhuber Anna[1,2], Jandl Katharina[1,3], Biasin Valentina[1,2], Fließer Elisabeth[1], Valzano Francesco[1], Marsh Leigh M[1], Krolczik Christina[4], Olschewski Andrea[1,5], Wilhelm Jochen[6], Toller Wolfgang[5], Heinemann Akos[3], Olschewski Horst[1,7], Wygrecka Malgorzata[4], Kwapiszewska Grazyna[1,2,8].

[1] Ludwig Boltzmann Institute for Lung Vascular Research Graz, Austria.

[2] Otto Loewi Research Center, Division of Physiology, Medical University of Graz, Graz, Austria.

[3] Otto Loewi Research Center, Division of Pharmacology, Medical University of Graz, Graz, Austria.

[4] Center for Infection and Genomics of the Lung, Universities of Giessen and Marburg Lung Center, Giessen, Germany. Member of the German Center for Lung Research.

[5] Department of Anaesthesiology and Intensive Care Medicina, Medical University of Graz, Graz, Austria.

[6] Department of Internal Medicine, Universities of Giessen and Marburg Lung Center, Giessen, Germany.

[7] Division of Pulmonology, Department of Internal Medicine, Medical University of Graz, Graz, Austria.

[8] Institute for Lung Health (ILH), Justus Liebig University, Giessen, Germany

*Corresponding author:

Grazyna Kwapiszewska

Ludwig Boltzmann Institute for Lung Vascular Research

Neue Stiftingtalstrasse 6/VI

8010 Graz, Austria

Phone number: +43 316 385-72918

E-mail: Grazyna.Kwapiszewska@lvr.lbg.ac.at

Funding: Pirfenidone was provided by HOFFMANN-LA ROCHE who also financially supported this study. EF and FV were funded by the Austrian Research Promotion Agency (FFG, project number: 34926649 and 874229) and trained within the frame of the PhD program Molecular Medicine of the Medical University of Graz. LMM is supported by FWF grant (KLIF 884-B) and the Austrian Research Promotion Agency (FFG, project number: 870904).

Declarations of Interest: AH has received remunerations from AstraZeneca for lecture activities; grants from Austrian Science Funds, FWF. HO received consulting fees from Actelion, Bayer AG, Böhringer Ingelheim, Inventiva, Janssen Pharmaceutica, MSD (Merck Sharp & Dohme), payment for educational events from Böhringer Ingelheim and remunerations for participation on Advisory Boards from Bayer AG, Pfizer, MSD (Merck Sharp & Dohme) andIQVIA Biotech LLC, and is Deputy Director of the Ludwig Boltzmann Institute for Lung Vascular Research. GK is Director of LBI-LVR. All other authors have nothing to disclose.

Take home message: Pirfenidone worsens vascular and pulmonary dysfunction in a SSc-ILD mouse model due to its negative effects on primed endothelial cells and may lead to unfavourable effects in patients with underlying type 2 inflammation as seen in SSc-ILD.

ABSTRACT

Systemic sclerosis (SSc) is an autoimmune disease characterised by severe vasculopathy and fibrosis of various organs including the lung. Targeted treatment options for SSc-associated interstitial lung disease (SSc-ILD) are scarce. Here we assessed the effects of pirfenidone in a mouse model of SSc-ILD.

Pulmonary function, inflammation and collagen deposition in response to pirfenidone were assessed in Fra-2-overexpressing (Fra-2 TG) and bleomycin-treated mice. In Fra-2 TG mice, lung transcriptome was analysed after pirfenidone treatment. *In vitro,* pirfenidone effects on human eosinophil and endothelial cell function were analysed using flow cytometry-based assays and electric cell-substrate impedance measurements, respectively.

Pirfenidone treatment attenuated pulmonary remodelling in the bleomycin-model, but aggravated pulmonary inflammation, fibrosis, and vascular remodelling in Fra-2 TG mice. Pirfenidone increased interleukin (IL)-4 levels and eosinophil numbers in lung tissue of Fra-2 TG mice without directly affecting eosinophil activation and migration *in vitro*. A pronounced immune response with high levels of cytokines/chemokines and disturbed endothelial integrity with low VE-cadherin levels were observed in pirfenidone-treated Fra-2 TG mice. In contrast, eosinophil, IL-4 and VE-cadherin levels were unchanged in bleomycin-treated mice and not influenced by pirfenidone. *In vitro*, pirfenidone exacerbated the IL-4 induced reduction of endothelial barrier resistance leading to higher leukocyte transmigration.

This study shows that anti-fibrotic properties of pirfenidone may be overruled by unwanted interactions with pre-injured endothelium in a setting of high Th2 inflammation in a model of SSc-ILD. Careful ILD patient phenotyping may be required to exploit benefits of pirfenidone while avoiding therapy failure and additional lung damage in some patients.

INTRODUCTION

SSc is an autoimmune disease leading to severe vasculopathy and fibrosis of various organs. It is characterized by vascular and fibrotic abnormalities, due to dysregulation of innate and adaptive immunity leading to high levels of inflammatory and pro-fibrotic mediators such as interleukin (IL)-1, IL-6, tumour necrosis factor α (TNFα) or transforming growth factor β (TGFβ), as well as the Th2 cytokines IL-4 and IL-13 [1, 2]. A growing body of evidence highlights SSc as a vascular disease with a prominent role of endothelial dysfunction. Endothelial cells and blood vessels seem to be the initial target of injury in all organs affected by the disease [3, 4]. Lung involvement, leading to interstitial lung disease in SSc (SSc-ILD) is very frequent and accounts for the majority of SSc-associated deaths [5, 6]. The underlying pathomechanisms are not fully elucidated, therefore disease-modifying treatment options for SSc-ILD are limited and therapy is mostly confined to systemic immunosuppression [7, 8]. The tyrosine kinase inhibitor nintedanib, previously used for the treatment of idiopathic pulmonary fibrosis (IPF), was only recently approved for the treatment of rapidly progressive SSc-ILD [9].

A second anti-fibrotic drug, pirfenidone, has long been discussed for SSc-ILD therapy. Pirfenidone reduces pro-inflammatory and fibrotic responses, by decreasing levels of inflammatory mediators and growth factors such as IL-1β or TGF-β, as shown in multiple cell culture studies, animal models and in IPF patients [10–14]. Although pirfenidone treatment does not cure IPF, it delays the decline in forced vital capacity and disease progression [12, 15]. While pirfenidone is approved as IPF treatment, it is not approved for other forms of pulmonary fibrosis (PF).

The RELIEF study investigated the effects of pirfenidone in patients with non-IPF progressive fibrotic ILD but was prematurely terminated due to slow enrolment [16]. In this study, pirfenidone delayed the decline in forced vital capacity without a significant increase in adverse effects. However, due to low patient numbers, subgroup analysis for SSc-ILD was

not possible [16]. Therefore, the question remains open whether SSc-ILD patients may benefit from pirfenidone treatment or whether they may be prone to adverse effects.

Here we tested the hypothesis that pirfenidone might be beneficial in SSc-ILD due to its anti-inflammatory and anti-fibrotic effects, by applying a mouse model overexpressing the AP-1 transcription factor Fos-related antigen-2 (Fra-2 transgene/TG) [17]. This model recapitulates major features of human SSc, such as early alterations of the vasculature with EC apoptosis [18], vascular remodelling [19] and development of pulmonary hypertension (preceding the onset of fibrosis), systemic inflammation [17, 20, 21] and fibrosis of skin and other internal organs, including the lungs [17, 22, 23]. Similar to SSc patients, Fra-2 TG mice have high levels of inflammatory mediators such as IL-1β and IL-6, and of Th2 cytokines such as IL-4 and IL-13 [1, 2, 17, 20], thus representing a valuable model to test drug-candidates for SSc-ILD patients.

In contrast to our expectations, pirfenidone aggravated the vascular and pulmonary phenotype in the Fra-2 mouse model of SSc-ILD. We provide evidence that in certain/specific inflammatory settings, pirfenidone may have detrimental effects on endothelial cell function and lung permeability.

MATERIAL AND METHODS

A detailed description of all methods is provided in the online data supplement.

Animal experiments

Female Fra-2 overexpressing/transgenic (Fra-2 TG) mice and wild-type (WT) littermates were maintained under specific pathogen free conditions in isolated ventilated cages with 12-hour light/dark cycles. All animal experiments met EU guidelines 2010/63/EU and were approved by the local authorities (Austrian Ministry of Education, Science and Culture). Bleomycin was given intra-tracheally at a dose of 0.8 units per kg bodyweight as described previously [24, 25]. Pirfenidone treatment protocol was adapted from previous publications [26] and incorporated into standard laboratory chow at 2.8 mg/g (Sniff, Soest, Germany). Pirfenidone was provided by HOFFMANN-LA ROCHE. Food was weighed regularly and mean pirfenidone uptake was calculated. Mean pirfenidone uptake was approximately 400 mg/kg bodyweight per day, a frequently used dosage in mouse studies, leading to pirfenidone exposure ratios and plasma concentrations similar to those in patients treated with pirfenidone [10, 27, 28]. Pirfenidone treatment of Fra-2 TG and WT mice was performed in two independent experiments with five to eight mice per group. Schematic representations of Fra-2 TG and bleomycin experiments are shown in Figures 1A and 5A, respectively.

RESULTS

Pirfenidone aggravates pulmonary remodelling in the Fra-2 TG mouse model

Eleven- to 12-week-old Fra-2 TG and WT mice received pirfenidone-supplemented food over the course of eight weeks (Figure 1A). As compared to mice on standard chow, pirfenidone treatment worsened lung function in Fra-2 TG mice, as indicated by decreased quasi-static compliance and significantly increased tissue damping, a parameter related to tissue resistance (Figure 1B). Increased collagen deposits were observed predominantly in perivascular regions of the lungs of Fra-2 TG mice (Figure S1). Collagen quantification by western blot analysis and hydroxyproline measurements revealed significantly elevated collagen levels in the lungs of pirfenidone-treated Fra-2 TG mice as compared to WT control mice (Figure 1C and 1D). In addition to parenchymal alterations, Fra-2 TG mice had enhanced muscularisation of small pulmonary vessels, which was aggravated upon pirfenidone treatment (Figure 1E and 1F). This indicates a negative influence of pirfenidone on the pulmonary circulation. Of note, pirfenidone did not affect lung function, pulmonary architecture, collagen deposition or vessel muscularisation in WT mice.

Pirfenidone treatment increases inflammatory infiltration and eosinophilia in Fra-2 TG mice

As previously shown [17, 20, 21], Fra-2 TG mice had elevated levels of inflammatory cells in the bronchoalveolar lavage fluid (BALF) (Figure 2A), which was further exacerbated by pirfenidone (Figure 2A). While almost all inflammatory cell populations were increased in the BALF (Figure 2B), alterations in the lung tissue were dominated by increased eosinophil levels (Figure 2C-E). In addition, gene expression and protein levels of IL-4 were elevated in the lungs of Fra-2 TG mice (Figure 2F, G). Again, pirfenidone did not alter the inflammatory profile or lung function in WT mice, indicating that pirfenidone by itself has no harmful effects on the healthy lung.

Of note, intranasal application of the glucocorticoid budesonide in Fra-2 TG mice ameliorated pulmonary inflammation, improved lung function [21] and decreased collagen deposition in

the lung parenchyma (Figure S2). This highlights the role of inflammation in the development of pulmonary fibrosis in this mouse model.

To investigate whether increased influx of eosinophils into the lung tissue might be due to direct effects of pirfenidone on eosinophils, we analysed stimulation-induced shape change, chemotaxis, reactive oxygen species (ROS) production and survival of human eosinophils isolated from blood in response to pirfenidone. Pirfenidone alone did not affect eosinophil activation as measured by shape change (Figure S3A) or reactive oxygen species production (Figure S3B). Eotaxin-induced shape change and chemotaxis remained unaltered by pirfenidone pre-treatment (Figure S3CD, and Figure S3D). Survival analysis showed that pirfenidone, alone or in combination with pro-survival factor IL-5, had no influence on eosinophil longevity *in vitro* (Figure S3E). In summary, pirfenidone did not alter eosinophil properties or function by its own, nor modulated eotaxin or IL-5 mediated effects on shape change, chemotaxis, or survival. Therefore, increased eosinophil abundance in the lungs of pirfenidone-treated Fra-2 TG mice cannot be explained by direct pirfenidone effects on eosinophils.

Transcriptomic profiling highlights inflammatory pathways upregulated upon pirfenidone treatment in Fra-2 TG mice

We next sought to describe the molecular processes induced by pirfenidone, that may explain the increased eosinophil numbers and worsened phenotype in Fra-2 TG mice. To this end, we performed transcriptional profiling of lung tissue from Fra-2 TG mice with and without eight weeks of pirfenidone treatment (Figure 1A and 3A). The top ten significantly up- or down-regulated genes, as defined by absolute Log-fold-change (LogFC) (Figure 3B), highlighted main changes in the lung. Several genes associated with mucosal immunity (BPI Fold Containing Family B Member 1, Bpifb1) or epithelial repair (Trefoil factor 2, Tff2) and function (Chloride Channel Accessory 1, Clca1) were downregulated, possibly indicating increased epithelial damage in Fra-2 TG mice following pirfenidone treatment. Within the strongest upregulated genes, most genes were linked to innate immunity (interferon

activated gene 202B, Ifi202b; ubiquitin D, Ubd; tripartite motif containing 12A, Trim12a; aconitate decarboxylase 1, Acod1; CC-chemokine ligand 1, Ccl1), to eosinophils (glyoxalase domain containing 5, Glod5) and to inflammatory diseases (cell adhesion molecule L1 like, Chl1, Acod1) (Figure 3B). Two of the top ten upregulated genes were also connected to an IPF-specific gene signature (cholecystokinin, Cck; and cell adhesion molecule L1 like, Chl1) [29]. These data point towards a dysregulation of the immune response and concomitant lung injury upon pirfenidone treatment in Fra-2 mice.

Gene enrichment analysis showed significant overrepresentation of altered gene expression in inflammatory pathways, such as chemotaxis and migration of lymphocytes, eosinophils and neutrophils, and the regulation thereof (Figure 3C). The top ten most significant gene ontologies were marked by the increased expression of chemokines such as Ccl1, Ccl2, Ccl3, Ccl4, Ccl7, Cxcl9 and Cxcl10 (Figure 3C). Unbiased hierarchical clustering of all genes of the two main parent gene ontologies, namely Cytokine-mediated signalling pathway (GO:0019221 – orange background, Figure 3D) and Leukocyte migration (GO:0050900 – green background, Figure 3E), showed clear separation of Fra-2 TG lung homogenates of mice with pirfenidone treatment compared to Fra-2 TG mice without pirfenidone treatment. In addition to upregulation of inflammatory cytokines such as Il-4, Ccl2/3/4 and transcription factors, such as Stat1/2 (Figure 3D, E), numerous endothelial cell junction or cell-contact proteins such as Ceacam1 (Carcinoembryonic Antigen-Related Cell Adhesion Molecule 1), Add2 (Adducin 2) or integrins (Itga3, Itga4) were downregulated (Figure 3E).

Pirfenidone leads to aggravated loss of VE-cadherin in Fra-2 TG mice

Inflammatory cell recruitment strongly depends on interactions of inflammatory and endothelial cells, enabling adhesion, rolling and transmigration through the endothelial cell layer. As expression of several endothelial cell junction proteins was decreased (Figure 3E), we investigated in detail whether the exaggerated inflammatory response induced by pirfenidone in Fra-2 TG mice was due to an effect on the endothelium. In our transcriptomic dataset, expression of many genes within the KEGG pathway “Leukocyte transendothelial

extravasation" (mmu04670) were altered, including a significant downregulation of vascular endothelial cadherin (VE-cadherin/Cadherin 5, Cdh5) (Figure 4A). Indeed, we could confirm a downregulation of Cdh5 gene expression in Fra-2 TG, but not WT mice, following pirfenidone treatment (Figure 4B). *Cdh5* was already lower in Fra-2 TG compared to WT mice without treatment (Figure 4B), pointing towards a disturbed cell barrier in the lungs of this mouse model. Immunofluorescence staining confirmed this observation. WT mice showed a clear VE-cadherin/Cdh5 staining of capillaries with and without pirfenidone treatment (Figure 4C), whereas the immunofluorescence signal was diffuse in Fra-2 TG lungs even without pirfenidone. Pirfenidone treatment further decreased signal intensity in Fra-2 TG lungs (Figure 4C). This may indicate disturbed endothelial barrier integrity and consequent inflammatory cell infiltration in the lungs of Fra-2 TG mice compared to WT mice, an effect further potentiated by pirfenidone treatment. Indeed, VE-cadherin expression negatively correlated with inflammatory cell counts in the BAL (Figure 4D).

Pirfenidone ameliorates pulmonary remodelling in bleomycin-induced lung fibrosis

To investigate whether pirfenidone effects seen in the Fra-2 TG mouse model of SSc-ILD may also be observed in another PF model, we investigated the pirfenidone response in a mouse model of bleomycin-induced lung fibrosis. Similar to the experimental design above, control or bleomycin treated mice received chow supplemented with or without pirfenidone (Figure 5A). As expected, bleomycin led to a decline in lung function, however, pirfenidone treatment had no effect on pulmonary compliance and tissue resistance, irrespective of bleomycin or saline pre-treatment (Figure 5B). Hydroxyproline analysis revealed a significant decrease in collagen levels in bleomycin-treated mice following pirfenidone administration (Figure 5C). We previously reported vascular remodelling with increased muscularisation of small parenchymal vessels in bleomycin-induced lung fibrosis [24]. This vascular remodelling was ameliorated by pirfenidone in bleomycin-treated mice (Figure 5D).

Pirfenidone did not alter inflammatory cell counts in the BALF of bleomycin- or saline-treated mice (Figure 5E). The number of eosinophils in the BALF of bleomycin-treated mice was

unaltered compared to the saline group and not influenced by pirfenidone treatment (Figure 5F). Unbiased hierarchical clustering of inflammatory cell populations clearly separated saline and bleomycin groups; however, no clustering was observed according to pirfenidone treatment (Figure 5G). Furthermore, both IL-4 and VE-cadherin expression levels were unaffected by pirfenidone treatment in the lungs of bleomycin mice (Figure 5H and 5I). Cumulatively, our data indicate that although lung function was not improved by pirfenidone, application of this drug led to reduced collagen deposition and vascular remodelling in the lungs of bleomycin-treated mice. Importantly, no worsening of pulmonary inflammation was observed.

Pirfenidone worsens cell barrier function in pre-primed human microvascular endothelial cells

To elucidate whether increased inflammatory cell recruitment after pirfenidone treatment *in vivo* was linked to downregulation of VE-cadherin and disturbance of endothelial barrier function, we monitored the resistance of human lung microvascular endothelial cells (HMVEC) in response to pirfenidone. Pirfenidone or its vehicle control (DMSO) alone did not affect HMVEC resistance (Figure 6A). As IL-4 is a potent Th2 cytokine leading to increased permeability of endothelial cells [30] and as it was significantly upregulated in Fra-2 TG mice (Figure 2F, G, we speculated that priming of endothelial cells through inflammatory factors, such as IL-4, may lead to exaggerated barrier disturbances upon pirfenidone exposure. Pre-treatment of HMVEC with IL-4 led to a steady decrease of barrier function over a time period of 600 min (Figure 6B). When challenging IL-4 primed HMVEC with pirfenidone, the loss of endothelial cell resistance was aggravated and observed at earlier time points than after IL-4 alone or IL-4 with vehicle control DMSO (Figure 6B and 6C). A significant drop in resistance was visible after ten min of combined treatment with IL-4 and pirfenidone, as compared to IL-4 treatment alone or with DMSO vehicle control (Figure 6D). Furthermore, the IL-4-induced reduction in barrier resistance two h post-treatment was aggravated by pirfenidone (Figure 6E).

In order to investigate whether the loss of barrier function induced by pirfenidone in an IL-4 dominated environment could contribute to the increased inflammatory cell recruitment observed in pirfenidone treated Fra-2 TG animals (Figure 2), we performed an *in vitro* trans-endothelial migration assay (Figure 6F). The presence of an endothelial monolayer strongly reduced polymorphonucelar leukocyte (PMNL) chemotaxis (Figure 6G). Pre-treatment of endothelial cells with IL-4 increased the serum-induced endothelial-transmigration of PMNL, which was further enhanced by stimulation with pirfenidone (Figure 6H). Of note, treatment of HMVEC with pirfenidone alone induced PMNL transmigration comparable to IL-4 treatment (Figure 6H). Taken together, pirfenidone led to loss of endothelial cell barrier function with concomitant increase in leukocyte transmigration in an IL-4 dominated environment *in vitro.* These alterations mimic the observed reduction of VE-cadherin expression and aggravated inflammatory infiltrates in the lungs of Fra-2 TG mice *in vivo*.

DISCUSSION

In this study, we describe the detrimental effects of pirfenidone on the pulmonary endothelium. Using a mouse model of SSc-ILD we show how pirfenidone exacerbates pulmonary inflammation, fibrosis and vascular remodelling. Pirfenidone is an approved treatment option for IPF but nor for other non-IPF interstitial lung diseases, such as SSc-ILD. First trials showed that pirfenidone was well tolerated in patients with SSc-ILD [31], yet several recent clinical trials reported no [32] or weak benefits [33]. Even though the recent RELIEF study did not show serious adverse events in progressive fibrotic interstitial lung diseases other than IPF, the study was prematurely terminated on the basis of an interim analysis for futility triggered by slow recruitment. Subgroup-analysis for SSc-ILD could not be performed as only eight SSc-ILD patients were enrolled [33]. As the role for pirfenidone in SSc-ILD is still unclear, animal models, such as the Fra-2 overexpressing/transgenic (Fra-2 TG) model, present a valuable tool to investigate its potential benefits or drawbacks in SSc-ILD.

Fra-2 TG mice are increasingly used as a model of SSc and SSc-related lung involvement. Fra-2 TG mice not only develop pulmonary fibrosis, but also reflect several important features of SSc-ILD, including vasculopathy with EC apoptosis and pulmonary hypertension [18, 19], systemic inflammation predominated by Th2 inflammation [17, 20, 21], followed by fibrosis of skin, lung and other organs [17, 22]. Therefore, this model enables pre-clinical investigations and proof-of-concept studies in the context on SSc-ILD. The Fra-2 TG model has already been applied to investigate the efficacy of nintedanib, another anti-fibrotic drug, recently approved for the treatment of SSc-ILD [23, 34]. In the Fra-2 TG model, nintedanib has been shown to ameliorate pulmonary vascular remodelling as well as parenchymal fibrosis, and additionally prevented endothelial cell apoptosis [23].

Here, we tested the effects of pirfenidone and provide evidence that pirfenidone enhances inflammation, parenchymal and vascular remodelling, as well as worsens lung function in the Fra-2 TG mouse model. In contrast, in the bleomycin-induced lung fibrosis model pirfenidone

treatment ameliorated pulmonary remodelling and collagen production, but it did not improve lung function parameters. This agrees with several studies reporting beneficial effects of pirfenidone on collagen deposition, however, there has been inconsistent reports describing its effects on lung function [10, 11]. This strong model specific response indicates an important interaction of pirfenidone with the underlying model specific pathomechanisms. This is of special interest as the molecular processes underlying IPF and non-IPF progressive fibrosing lung diseases such as SSc-ILD are diverse and poorly understood [35]. While cellular injury is considered a common trigger for both disease entities, the current paradigm points to injury of epithelial cells in IPF on the one hand, and endothelial cells in SSc-ILD on the other hand [35]. Furthermore, immune alterations in SSc-ILD compared to IPF are distinct. This is highlighted by IL-4 serum levels which are elevated in SSc-ILD, but not in IPF [36, 37]. In agreement with this, we could show that IL-4 expression levels were elevated in the Fra-2 TG mouse model of SSc-ILD, but not in the bleomycin-induced model of lung fibrosis.

This background information as well as the fact that negative effects of pirfenidone were only observed in Fra-2 TG but not in WT mice, triggered the hypothesis that these adverse effects of pirfenidone might be due to the primed/activated vascular endothelium in the inflammatory setting of Fra-2 TG mice.

Pathological changes of the peripheral vascular endothelium are central in SSc from early disease stages on, and include loss of adhesion junctions, barrier breakdown, vascular leakage and altered cell extravasation/migration [38, 39]. Although the initial trigger for endothelial injury in SSc remains unknown, inflammatory components could potentiate EC activation and dysfunction. Indeed, already in early SSc, immune cells migrate into the lungs and participate in remodelling of the vascular wall [40]. Unravelling the molecular mechanisms underlying vascular microleakage in SSc could therefore be of paramount importance to elucidate interactions with potential future therapeutics such as pirfenidone. Here, the Fra-2 TG is of particular importance as it closely reflects many aspects of SSc-ILD,

including early alterations of the vasculature which precede the onset of fibrosis [24]. Together with other models of PF, it might be a valuable tool to examine different aetiologies and pathomechanisms of ILDs and could help to develop more targeted and personalized treatment approaches.

Our transcriptomic analysis revealed that, in Fra-2 TG mice, pirfenidone activated several pathways involved in chemotaxis of granulocytes and lymphocytes. This was on the one hand due to the increased expression of chemoattractants, such as members of the C-C and C-X-C family of chemokines as well as classical cytokines such as IL-4 or IL-6, and on the other hand due to lower expression of genes involved in endothelial barrier formation (e.g., integrins or carcinoembryonic antigen-related cell adhesion molecule-1 (CEACAM1). Knockdown of CEACAM1 is known to modulate endothelial barrier leakiness, to increase leukocyte-endothelial interaction [41], and to enhance the development of cardiac fibrosis [42]. These observations support our hypothesis that the inflammatory status of this model primes the pulmonary endothelium for the loss of barrier integrity and increased susceptibility to injury.

Indeed, Fra-2 TG mice exhibit prominent, partially Th2-driven inflammation with high levels of IL-4 [17, 20]. Our findings and those of others demonstrated that IL-4 led to decreased endothelial barrier function [30]. Of note, similar effects were reported for IL-1β [43], another inflammatory cytokine, whose levels are elevated in this mouse model [20]. This suggests that the observed endothelial disturbances in Fra-2 TG mice are most likely not due to one specific mediator, but the entire inflammatory environment. Mechanistically, IL-1β led to reduced endothelial barrier function, due to the suppression of VE-cadherin/Cdh5 expression [43].

In line with this, we showed that Fra-2 TG mice exhibited lower expression of VE-cadherin and increased lung permeability compared to WT mice [44]. This decrease was even stronger in pirfenidone-treated animals. Of note, VE-cadherin levels were unaltered in bleomycin-treated as compared to saline-control mice, and pirfenidone did not affect VE-

cadherin expression in bleomycin-treated mice. VE-cadherin is a key component of endothelial adherens junctions and important for barrier integrity and vascular permeability [45]. Loss of VE-cadherin has been described in patients with SSc [46]. VE-cadherin is also downregulated in the lung in response to inflammatory stimuli causing decreased permeability that correlates with poor prognosis [43, 47, 48]. Loss of VE-cadherin was shown in diverse mouse models of fibrosis, underpinning its importance in EC homeostasis and thus attenuation of fibrosis development [49, 50].

Since vascular and endothelial alterations are a major disease component of SSc, it is vital to understand the mode of action of pirfenidone, in particular its effect on the endothelium. In the carefully balanced interactions between endothelium and immune system, pirfenidone might trigger a vicious cycle of endothelial injury and immune cell recruitment, leading to exacerbated damage of the endothelium. Based on our experimental data, we speculate that Th2-predominant eosinophilic inflammation and endothelial barrier disturbance may be triggers for unfavourable pirfenidone effects in patients. The clinical relevance of our findings is highlighted by case reports describing increased wheezing and cough, eosinophilic pneumonia, and increased numbers of lymphocytes and eosinophils after the administration of pirfenidone in IPF patients [51, 52, 53]. Assessment of IL-4 levels, eosinophilia and soluble VE-cadherin as a possible surrogate marker for endothelial barrier dysfunction, might therefore be useful tools to distinguish pirfenidone responders from patients at risk of disease exacerbation. However, no data on circulating VE-cadherin and IL-4/eosinophil levels in IPF patients following pirfenidone are available to date and whether they correlate with treatment response needs to be established in further studies.

A limitation of our study is that it is purely based on animal models and lacks clinical data. Nonetheless, it has valuable translational potential as the Fra-2 TG mouse model closely resembles human SSc-ILD and has been successfully used to assess the efficacy of nintedanib, recently approved for the treatment of SSc-ILD, or IL-13 blocking antibodies [21, 23, 33]. Further, our *in vitro* data confirmed the endothelial barrier loss upon pirfenidone

treatment in inflammatory settings seen *in vivo* in Fra-2 TG mice. In conclusion, this study shows that the well-established anti-fibrotic properties of pirfenidone may be overruled by unwanted interactions with pre-injured endothelium in a setting of high Th2 inflammation. Therefore, assessment of Th2 cytokine and eosinophil levels, together with markers of an activated/injured endothelium could be useful to discriminate patients at risk of adverse effects and potential disease exacerbations from patients that may benefit from pirfenidone treatment.

Acknowledgements

We would like to thank Bettina Schrenk, Thomas Fuchs, Hans-Peter Ziegler, Simone Tischler and Kathrin Rohrer for excellent technical support. We are grateful to the Institute for Molecular Pathology Vienna and Prof. Erwin Wagner for Fra-2 TG mice.

References

1. Shima Y. Cytokines Involved in the Pathogenesis of SSc and Problems in the Development of Anti-Cytokine Therapy. *Cells* 2021; 10.

2. Huang X-L, Wang Y-J, Yan J-W, Wan Y-N, Chen B, Li B-Z, Yang G-J, Wang J. Role of anti-inflammatory cytokines IL-4 and IL-13 in systemic sclerosis. *Inflammation Research* 2015; 64.

3. Mostmans Y, Cutolo M, Giddelo C, Decuman S, Melsens K, Declercq H, Vandecasteele E, de Keyser F, Distler O, Gutermuth J, Smith V. The role of endothelial cells in the vasculopathy of systemic sclerosis: A systematic review. *Autoimmunity Reviews* 2017; 16.

4. Matucci-Cerinic M, Kahaleh B, Wigley FM. Review: Evidence That Systemic Sclerosis Is a Vascular Disease. *Arthritis & Rheumatism* 2013; 65.

5. Volkmann ER, Fischer A. Update on morbidity and mortality in systemic sclerosis–related interstitial lung disease. *Journal of Scleroderma and Related Disorders* 2021; 6.

6. Elhai M, Meune C, Boubaya M, Avouac J, Hachulla E, Balbir-Gurman A, Riemekasten G, Airò P, Joven B, Vettori S, Cozzi F, Ullman S, Czirják L, Tikly M, Müller-Ladner U, Caramaschi P, Distler O, Iannone F, Ananieva LP, Hesselstrand R, Becvar R, Gabrielli A, Damjanov N, Salvador MJ, Riccieri V, Mihai C, Szücs G, Walker UA, Hunzelmann N, Martinovic D, et al. Mapping and predicting mortality from systemic sclerosis. *Annals of the Rheumatic Diseases* 2017; 76.

7. Giacomelli R, Liakouli V, Berardicurti O, Ruscitti P, di Benedetto P, Carubbi F, Guggino G, di Bartolomeo S, Ciccia F, Triolo G, Cipriani P. Interstitial lung disease in systemic sclerosis: current and future treatment. *Rheumatology International* 2017; 37.

8. Koutroumpas A, Ziogas A, Alexiou I, Barouta G, Sakkas LI. Mycophenolate mofetil in systemic sclerosis-associated interstitial lung disease. *Clinical Rheumatology* 2010; 29.

9. Seibold JR, Maher TM, Highland KB, Assassi S, Azuma A, Hummers LK, Costabel U, von Wangenheim U, Kohlbrenner V, Gahlemann M, Alves M, Distler O. Safety and tolerability of nintedanib in patients with systemic sclerosis-associated interstitial lung disease: data from the SENSCIS trial. *Annals of the Rheumatic Diseases* 2020; 79.

10. Schaefer CJ, Ruhrmund DW, Pan L, Seiwert SD, Kossen K. Antifibrotic activities of pirfenidone in animal models. *European Respiratory Review* 2011; 20.

11. Oku H, Shimizu T, Kawabata T, Nagira M, Hikita I, Ueyama A, Matsushima S, Torii M, Arimura A. Antifibrotic action of pirfenidone and prednisolone: Different effects on pulmonary cytokines and growth factors in bleomycin-induced murine pulmonary fibrosis. *European Journal of Pharmacology* 2008; 590.

12. Takeda Y, Tsujino K, Kijima T, Kumanogoh A. Efficacy and safety of pirfenidone for idiopathic pulmonary fibrosis. *Patient Preference and Adherence* 2014; .

13. Didiasova M, Singh R, Wilhelm J, Kwapiszewska G, Wujak L, Zakrzewicz D, Schaefer L, Markart P, Seeger W, Lauth M, Wygrecka M. Pirfenidone exerts antifibrotic effects through inhibition of GLI transcription factors. *The FASEB Journal* 2017; 31.

14. Kwapiszewska G, Gungl A, Wilhelm J, Marsh LM, Thekkekara Puthenparampil H, Sinn K, Didiasova M, Klepetko W, Kosanovic D, Schermuly RT, Wujak L, Weiss B, Schaefer L, Schneider M, Kreuter M, Olschewski A, Seeger W, Olschewski H, Wygrecka M. Transcriptome profiling reveals the complexity of pirfenidone effects in idiopathic pulmonary fibrosis. *European Respiratory Journal* 2018; 52.

15. Noble PW, Albera C, Bradford WZ, Costabel U, du Bois RM, Fagan EA, Fishman RS, Glaspole I, Glassberg MK, Lancaster L, Lederer DJ, Leff JA, Nathan SD, Pereira CA,

Swigris JJ, Valeyre D, King TE. Pirfenidone for idiopathic pulmonary fibrosis: analysis of pooled data from three multinational phase 3 trials. *European Respiratory Journal* 2016; 47.

16. Behr J, Prasse A, Kreuter M, Johow J, Rabe KF, Bonella F, Bonnet R, Grohe C, Held M, Wilkens H, Hammerl P, Koschel D, Blaas S, Wirtz H, Ficker JH, Neumeister W, Schönfeld N, Claussen M, Kneidinger N, Frankenberger M, Hummler S, Kahn N, Tello S, Freise J, Welte T, Neuser P, Günther A, Behr J, Kreuter M, Johow J, et al. Pirfenidone in patients with progressive fibrotic interstitial lung diseases other than idiopathic pulmonary fibrosis (RELIEF): a double-blind, randomised, placebo-controlled, phase 2b trial. *The Lancet Respiratory Medicine* 2021; 9.

17. Eferl R, Hasselblatt P, Rath M, Popper H, Zenz R, Komnenovic V, Idarraga M-H, Kenner L, Wagner EF. Development of pulmonary fibrosis through a pathway involving the transcription factor Fra-2/AP-1. *Proceedings of the National Academy of Sciences* 2008; 105.

18. Maurer B, Busch N, Jüngel A, Pileckyte M, Gay RE, Michel BA, Schett G, Gay S, Distler J, Distler O. Transcription Factor Fos-Related Antigen-2 Induces Progressive Peripheral Vasculopathy in Mice Closely Resembling Human Systemic Sclerosis. *Circulation* 2009; 120.

19. Biasin V, Marsh LM, Egemnazarov B, Wilhelm J, Ghanim B, Klepetko W, Wygrecka M, Olschewski H, Eferl R, Olschewski A, Kwapiszewska G. Meprin β , a novel mediator of vascular remodelling underlying pulmonary hypertension. *The Journal of Pathology* 2014; 233.

20. Birnhuber A, Crnkovic S, Biasin V, Marsh LM, Odler B, Sahu-Osen A, Stacher-Priehse E, Brcic L, Schneider F, Cikes N, Ghanim B, Klepetko W, Graninger W, Allanore Y, Eferl R, Olschewski A, Olschewski H, Kwapiszewska G. IL-1 receptor blockade skews

inflammation towards Th2 in a mouse model of systemic sclerosis. *European Respiratory Journal* 2019; 54.

21. Gungl A, Biasin V, Wilhelm J, Olschewski A, Kwapiszewska G, Marsh LM. Fra2 Overexpression in Mice Leads to Non-allergic Asthma Development in an IL-13 Dependent Manner. *Frontiers in Immunology* 2018; 9.

22. Reich N, Maurer B, Akhmetshina A, Venalis P, Dees C, Zerr P, Palumbo K, Zwerina J, Nevskaya T, Gay S, Distler O, Schett G, Distler JHW. The transcription factor Fra-2 regulates the production of extracellular matrix in systemic sclerosis. *Arthritis & Rheumatism* 2010; 62.

23. Huang J, Maier C, Zhang Y, Soare A, Dees C, Beyer C, Harre U, Chen C-W, Distler O, Schett G, Wollin L, Distler JHW. Nintedanib inhibits macrophage activation and ameliorates vascular and fibrotic manifestations in the Fra2 mouse model of systemic sclerosis. *Annals of the Rheumatic Diseases* 2017; 76.

24. Biasin V, Crnkovic S, Sahu-Osen A, Birnhuber A, el Agha E, Sinn K, Klepetko W, Olschewski A, Bellusci S, Marsh LM, Kwapiszewska G. PDGFRα and αSMA mark two distinct mesenchymal cell populations involved in parenchymal and vascular remodeling in pulmonary fibrosis. *American Journal of Physiology-Lung Cellular and Molecular Physiology* 2020; 318: L684–L697.

25. Bordag N, Biasin V, Schnoegl D, Valzano F, Jandl K, Nagy BM, Sharma N, Wygrecka M, Kwapiszewska G, Marsh LM. Machine Learning Analysis of the Bleomycin Mouse Model Reveals the Compartmental and Temporal Inflammatory Pulmonary Fingerprint. *iScience* 2020; 23: 101819.

26. Kehrer JP, Margolin SB. Pirfenidone diminishes cyclophosphamide-induced lung fibrosis in mice. *Toxicology Letters* 1997; 90.

27. Kakugawa T, Mukae H, Hayashi T, Ishii H, Abe K, Fujii T, Oku H, Miyazaki M, Kadota J, Kohno S. Pirfenidone attenuates expression of HSP47 in murine bleomycin-induced pulmonary fibrosis. *European Respiratory Journal* 2004; 24: 57–65.

28. Kehrer JP, Margolin SB. Pirfenidone diminishes cyclophosphamide-induced lung fibrosis in mice. *Toxicology Letters* 1997; 90: 125–132.

29. Wang Y, Yella J, Chen J, McCormack FX, Madala SK, Jegga AG. Unsupervised gene expression analyses identify IPF-severity correlated signatures, associated genes and biomarkers. *BMC Pulmonary Medicine* 2017; 17.

30. Skaria T, Burgener J, Bachli E, Schoedon G. IL-4 Causes Hyperpermeability of Vascular Endothelial Cells through Wnt5A Signaling. *PLOS ONE* 2016; 11.

31. Khanna D, Albera C, Fischer A, Khalidi N, Raghu G, Chung L, Chen D, Schiopu E, Tagliaferri M, Seibold JR, Gorina E. An Open-label, Phase II Study of the Safety and Tolerability of Pirfenidone in Patients with Scleroderma-associated Interstitial Lung Disease: the LOTUSS Trial. *The Journal of Rheumatology* 2016; 43.

32. Acharya N, Sharma SK, Mishra D, Dhooria S, Dhir V, Jain S. Efficacy and safety of pirfenidone in systemic sclerosis-related interstitial lung disease—a randomised controlled trial. *Rheumatology International* 2020; 40.

33. Behr J, Prasse A, Kreuter M, Johow J, Rabe KF, Bonella F, Bonnet R, Grohe C, Held M, Wilkens H, Hammerl P, Koschel D, Blaas S, Wirtz H, Ficker JH, Neumeister W, Schönfeld N, Claussen M, Kneidinger N, Frankenberger M, Hummler S, Kahn N, Tello S, Freise J, Welte T, Neuser P, Günther A, Behr J, Kreuter M, Johow J, et al. Pirfenidone in patients with progressive fibrotic interstitial lung diseases other than idiopathic pulmonary fibrosis (RELIEF): a double-blind, randomised, placebo-controlled, phase 2b trial. *The Lancet Respiratory Medicine* 2021; 9.

34. Distler O, Highland KB, Gahlemann M, Azuma A, Fischer A, Mayes MD, Raghu G, Sauter W, Girard M, Alves M, Clerisme-Beaty E, Stowasser S, Tetzlaff K, Kuwana M, Maher TM. Nintedanib for Systemic Sclerosis–Associated Interstitial Lung Disease. *New England Journal of Medicine* 2019; 380.

35. Herzog EL, Mathur A, Tager AM, Feghali-Bostwick C, Schneider F, Varga J. Review: Interstitial Lung Disease Associated With Systemic Sclerosis and Idiopathic Pulmonary Fibrosis: How Similar and Distinct? *Arthritis & Rheumatology* 2014; 66.

36. Needleman BW, Wigley FM, Stair RW. Interleukin-1, Interleukin-2, Interleukin-4, Interleukin-6, Tumor Necrosis Factor α, and Interferon-γ Levels in Sera from Patients With Scleroderma. *Arthritis & Rheumatism* 1992; 35.

37. Tsoutsou PG, Gourgoulianis KI, Petinaki E, Germenis A, Tsoutsou AG, Mpaka M, Efremidou S, Molyvdas P-A. Cytokine levels in the sera of patients with idiopathic pulmonary fibrosis. *Respiratory Medicine* 2006; 100.

38. Chora I, Guiducci S, Manetti M, Romano E, Mazzotta C, Bellando-Randone S, Ibba-Manneschi L, Matucci-Cerinic M, Soares R. Vascular biomarkers and correlation with peripheral vasculopathy in systemic sclerosis. *Autoimmunity Reviews* 2015; 14.

39. Bruni C, Frech T, Manetti M, Rossi FW, Furst DE, de Paulis A, Rivellese F, Guiducci S, Matucci-Cerinic M, Bellando-Randone S. Vascular Leaking, a Pivotal and Early Pathogenetic Event in Systemic Sclerosis: Should the Door Be Closed? *Frontiers in Immunology* 2018; 9.

40. FRECH TM, REVELO MP, DRAKOS SG, MURTAUGH MA, MARKEWITZ BA, SAWITZKE AD, LI DY. Vascular Leak Is a Central Feature in the Pathogenesis of Systemic Sclerosis. *The Journal of Rheumatology* 2012; 39.

41. Ghavampour S, Kleefeldt F, Bömmel H, Volland J, Paus A, Horst A, Pfeiffer V, Hübner S, Wagner N, Rueckschloss U, Ergün S. Endothelial barrier function is differentially regulated by CEACAM1-mediated signaling. *The FASEB Journal* 2018; 32.

42. MUTURI HT, GHADIEH HE, KHUDER SS, JASH S, ABU HELAL R, DANIELS NA, LIU J, PURI V, VAZQUEZ G, GUPTA R, NAJJAR SM. Loss of CEACAM1 in Endothelial Cells Contributes to the Development of Cardiac Fibrosis. *Diabetes* 2018; 67.

43. Xiong S, Hong Z, Huang LS, Tsukasaki Y, Nepal S, Di A, Zhong M, Wu W, Ye Z, Gao X, Rao GN, Mehta D, Rehman J, Malik AB. IL-1β suppression of VE-cadherin transcription underlies sepsis-induced inflammatory lung injury. *Journal of Clinical Investigation* 2020; 130.

44. Tabeling C, Wienhold S-M, Birnhuber A, Brack MC, Nouailles G, Kershaw O, Firsching TC, Gruber AD, Lienau J, Marsh LM, Olschewski A, Kwapiszewska G, Witzenrath M. Pulmonary fibrosis in Fra-2 transgenic mice is associated with decreased numbers of alveolar macrophages and increased susceptibility to pneumococcal pneumonia. *American Journal of Physiology-Lung Cellular and Molecular Physiology* 2021; 320.

45. Giannotta M, Trani M, Dejana E. VE-Cadherin and Endothelial Adherens Junctions: Active Guardians of Vascular Integrity. *Developmental Cell* 2013; 26.

46. Fleming JN, Shulman HM, Nash RA, Johnson PY, Wight TN, Gown A, Schwartz SM. Cutaneous Chronic Graft-Versus-Host Disease Does Not Have the Abnormal Endothelial Phenotype or Vascular Rarefaction Characteristic of Systemic Sclerosis. *PLoS ONE* 2009; 4: e6203.

47. Probst CK, Montesi SB, Medoff BD, Shea BS, Knipe RS. Vascular permeability in the fibrotic lung. *European Respiratory Journal* 2020; 56.

48. Herwig MC, Tsokos M, Hermanns MI, Kirkpatrick CJ, Müller AM. Vascular Endothelial Cadherin Expression in Lung Specimens of Patients with Sepsis-Induced Acute Respiratory Distress Syndrome and Endothelial Cell Cultures. *Pathobiology* 2013; 80.

49. Nikitopoulou I, Manitsopoulos N, Kotanidou A, Tian X, Petrovic A, Magkou C, Ninou I, Aidinis V, Schermuly RT, Kosanovic D, Orfanos SE. Orotracheal treprostinil administration attenuates bleomycin-induced lung injury, vascular remodeling, and fibrosis in mice. *Pulmonary Circulation* 2019; 9.

50. Yamaguchi I, Tchao BN, Burger ML, Yamada M, Hyodo T, Giampietro C, Eddy AA. Vascular Endothelial Cadherin Modulates Renal Interstitial Fibrosis. *Nephron Experimental Nephrology* 2012; 120.

51. Campainha S, Nogueira C, Costa F, Sanches A, Neves S. Not yet known side effects of pirfenidone in the treatment of idiopathic pulmonary fibrosis? *Revista Portuguesa de Pneumologia (English Edition)* 2016; 22.

52. Gomez DC, Mehrad B. Eosinophilic pneumonia associated with pirfenidone therapy. *European Respiratory Journal* 2016; 48.

53. Suda K, Kamiya K, Chiang B, Okada H, Mato N, Maekawa T, Komine M, Murata S, Ohtsuki M. A rare case of drug-induced hypersensitivity syndrome by pirfenidone for idiopathic pulmonary fibrosis. *Allergology International* 2018; 67.

Figure Legends

Figure 1: Pulmonary remodelling is worsened following pirfenidone treatment in Fra-2 TG mice. A) Schematic representation of pirfenidone (P) treatment in Fra-2 transgenic (TG) and wild-type (WT) mice. Lung function measurements and organ collection was performed in ~ 20-week-old mice after 8 weeks of pirfenidone treatment. (B) Lung function measurements showing quasi-static compliance (Cst) and Tissue dampening (G). (C) Western blot analysis and corresponding quantification of Collagen I (COL1) in lung homogenates of WT and TG mice with (+P) and without pirfenidone. α-tubulin (αTUB) served as loading control. One of two Western blots is shown. (D) Hydroxyproline measurement of collagen in lung tissue. Data are indicated as boxplots with dot plot overlays. Statistical analysis was performed using non-parametric Kruskal-Wallis testing with post analysis to compare specific groups. *p<0.05, **p<0.01, ***p<0.001. (E) Representative images of double immunohistochemical staining for von Willebrand factor (brown) and α-smooth muscle actin (purple). Scalebar = 10 µm. (F) Percentage of non-muscularised (non mus.), partially muscularised (part mus.) and fully muscularised (fully mus.) vessels below 100 µm in diameter. n=4 (TG) or n=6 (WT, WT+P and TG+ P). Data are shown as mean ± SD.

Figure 2: Pirfenidone increases inflammatory cell counts in the bronchoalveolar lavage (BAL) and eosinophilic infiltration into the lung tissue in Fra-2 TG mice. (A) Inflammatory cell count in the BAL of wild-type (WT) and Fra-2 transgenic (TG) mice with (+P) and without pirfenidone treatment. (B/C) Heat map representation with hierarchical clustering of relative proportions of inflammatory cell populations in BAL (B) and lung tissue (C) of WT and TG mice with (+P) and without pirfenidone treatment. Data were normalised using sqrt(sqrt(cellcount)); z-scores are shown. (D) Eosinophil cell count in BAL and lung tissue of WT and TG mice with (+P) and without pirfenidone treatment. (E) Chromotrop 2R staining of eosinophil granules (highlighted by arrowheads) in the lung tissue of WT and TG mice with and without pirfenidone treatment. Scalebar = 10 µm. (F) Quantitative real-time PCR analysis of *IL4* gene expression. (G) IL-4 protein content in lung tissue homogenates. Data are indicated as boxplots with dot plot overlays. Statistical analysis was performed

using non-parametric Kruskal-Wallis testing with post analysis to compare specific groups. *p<0.05, **p<0.01.

Figure 3: Transcriptomic profiling highlights inflammatory pathways upregulated upon pirfenidone treatment in Fra-2 TG mice. (A) Schematic representation of the experimental setup. (B) Volcano plot showing differential gene regulation in Fra-2 TG mouse lungs with (+P) and without pirfenidone. Top 10 regulated genes according to their LogFoldChange (LogFC) are labelled by name. (C) Top 10 significantly regulated gene ontologies (GO biological process) and their significantly regulated genes within the dataset. (D, E) Heatmap representation with hierarchical clustering of genes within the gene ontologies (D) GO:0019221 Cytokine-mediated signalling pathway and (E) GO:0050900 Leukocyte migration.

Figure 4: Pirfenidone leads to decreased VE-cadherin expression in the lungs of Fra-2 TG mice. (A) Schematic of the Kyoto Encyclopedia of Genes and Genomes (KEGG) pathway “Leukocyte transendothelial migration”. The log fold change of gene expression is indicated by colour, significance of regulation is indicated by box borders. (B) Quantitative real-time PCR analysis of VE-cadherin (*Cdh5*). Data are indicated as boxplots with dot plot overlays. Statistical analysis was performed using non-parametric Kruskal-Wallis testing with post analysis to compare specific groups. *p<0.05, **p<0.01, ***p<0.001. (C) Low and high magnification immunofluorescence images of VE-cadherin (Cdh5) and von Willebrand factor (Vwf) staining in lung tissue from wild-type (WT) and Fra-2 transgenic (TG) mice with (+P) and without pirfenidone treatment. Nuclear counterstain was performed using DAPI. Scalebar = 10 µm. (D) Spearman’s rank correlation analysis of inflammatory cells in the bronchoalveolar lavage fluid (BAL cell count) and Cdh5 expression.

Figure 5: Pirfenidone ameliorates pulmonary remodelling without affecting lung function and inflammation in a bleomycin-induced mouse model of pulmonary fibrosis. A) Schematic representation of pirfenidone (P) treatment in the bleomycin-induced mouse model of pulmonary fibrosis. Lung function measurements and organ collection was

performed 21 days after bleomycin and 14 days after pirfenidone treatment. (B) Lung function measurements showing quasi-static compliance (Cst) and Tissue dampening/resistance (G). (C) Hydroxyproline measurement of collagen in lung tissue of saline and bleomycin-treated mice with (+P) and without pirfenidone. Data are indicated as boxplots with dot plot overlays. Statistical analysis was performed using non-parametric Kruskal-Wallis testing with post analysis to compare specific groups. *p<0.05, **p<0.01, ***p<0.001. (D) Percentage of non-muscularised (non mus.), partially muscularised (part mus.) and fully muscularised (fully mus.) vessels below 100 µm in diameter. n=5 (Bleo) or n=7 (Bleo+P). Data are shown as mean ± SD. (E) Inflammatory cell and (F) eosinophil counts in the bronchoalveolar lavage (BAL) of bleomycin and saline-treated mice with (+P) and without pirfenidone treatment. (G) Heat map representation with hierarchical clustering of relative proportions of inflammatory cell populations in BAL of bleomycin and saline-treated mice with (+P) and without pirfenidone treatment. Data were normalised using sqrt(sqrt(cellcount)); z-scores are shown. (H and I) Quantitative real-time PCR analysis of *IL4* (H) and VE-cadherin (*Cdh5*, G) gene expression. Data are indicated as boxplots with dot plot overlays.

Figure 6: Priming with interleukin (IL)-4 sensitizes human lung microvascular endothelial cells (HMVECs) and leads to increased loss of barrier function and increased polymorphonuclear leukocyte (PMNL) transmigration upon pirfenidone treatment. (A) Electric Cell-substrate Impedance Sensing (ECIS) measurement of HMVEC barrier resistance in response to pirfenidone. DMSO and basal medium served as vehicle and negative control, respectively. (B) ECIS measurements of HMVEC barrier resistance in response to IL-4 alone compared to basal medium (vehicle control aqua dest.) (C) ECIS measurements of HMVEC barrier resistance in response to IL-4 in combination with pirfenidone or DMSO vehicle control. (D, E) Detailed analysis of (B) and (C) at 10 (D) and 120 min (E) post-treatment. Statistical analysis was performed using two-way ANOVA with multiple comparison testing. IL-4 effect: *p<0.05, **p<0.01, ***p<0.001; pirfenidone effect: $^{\#}$p<0.05. (F) Schematic representation of the transendothelial migration experimental setup.

Endothelial cells were cultured on 3 µm transmembrane inserts and polymorphonuclear leukocytes (PMNL, consisting of eosinophils and neutrophils) were allowed to migrate to 0 or 10% FBS, respectively, in the presence or absence of IL4 and/or pirfenidone (G) Transendothelial migration of PMNLs through 3 µm transwell insets with and without HMVEC monolayers in basal medium with 0% serum. (H) Transendothelial migration of PMNLs through established HMVEC monolayers in the presence of IL-4 and/or pirfenidone and corresponding vehicle controls. Statistical analysis was performed by one-way ANOVA with Dunnett's post-test using 0% serum with DMSO as control. *$p<0.05$, **$p<0.01$; T-test was used to compare IL-4 with and without pirfenidone treatment. $^{\#}$ $p<0.05$.

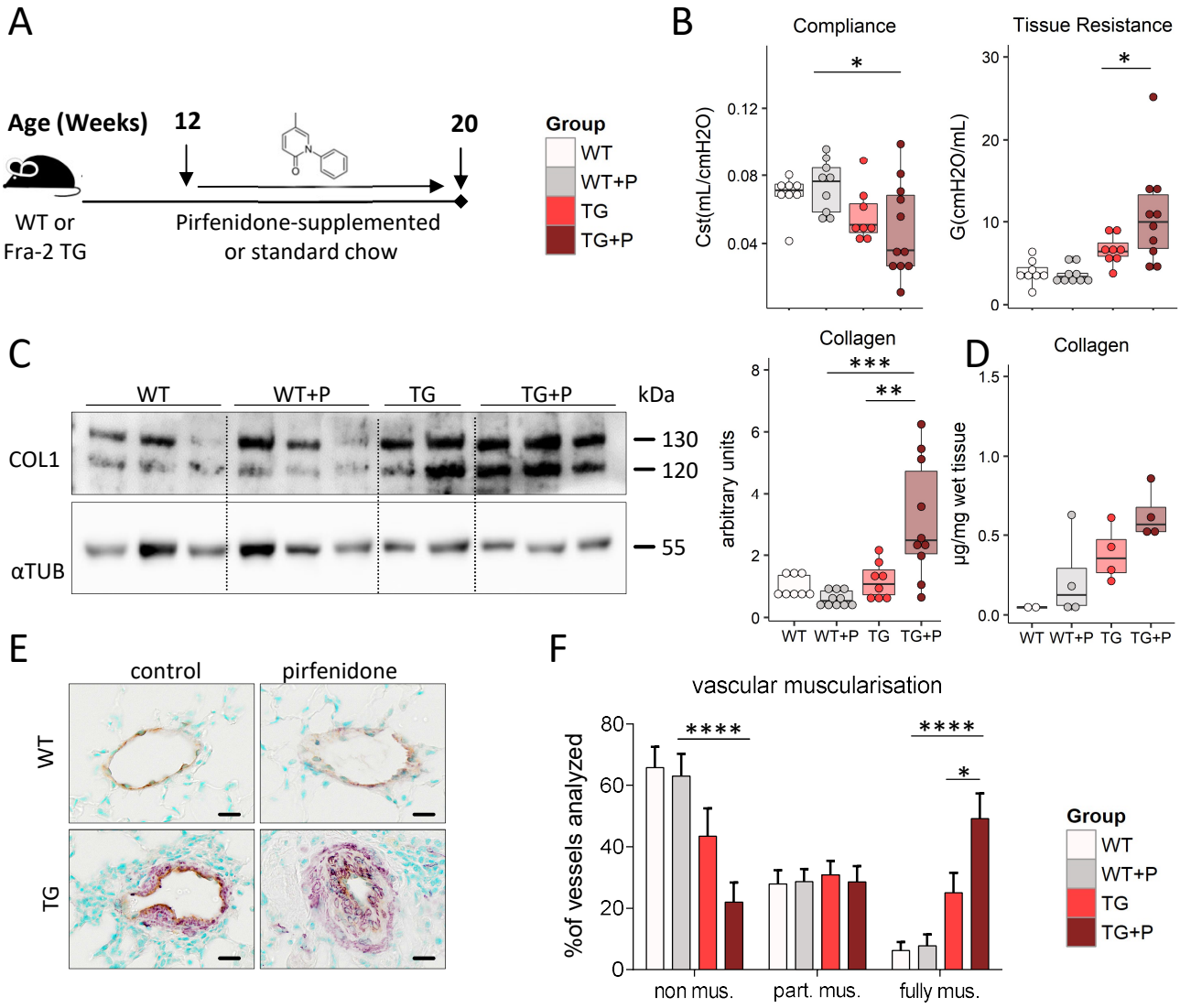
A
Age (Weeks)
12
20
WT or
Fra-2 TG
Pirfenidone-supplemented
or standard chow
Group
WT
WT+P
TG
TG+P
B
Compliance
Cst(mL/cmH2O)
Tissue Resistance
G(cmH2O/mL)
C
WT
WT+P
TG
TG+P
kDa
COL1
αTUB
130
120
55
Collagen
arbitrary units
D
Collagen
µg/mg wet tissue
E
control
pirfenidone
WT
TG
F
vascular muscularisation
%of vessels analyzed
non mus.
part. mus.
fully mus.
Group
WT
WT+P
TG
TG+P

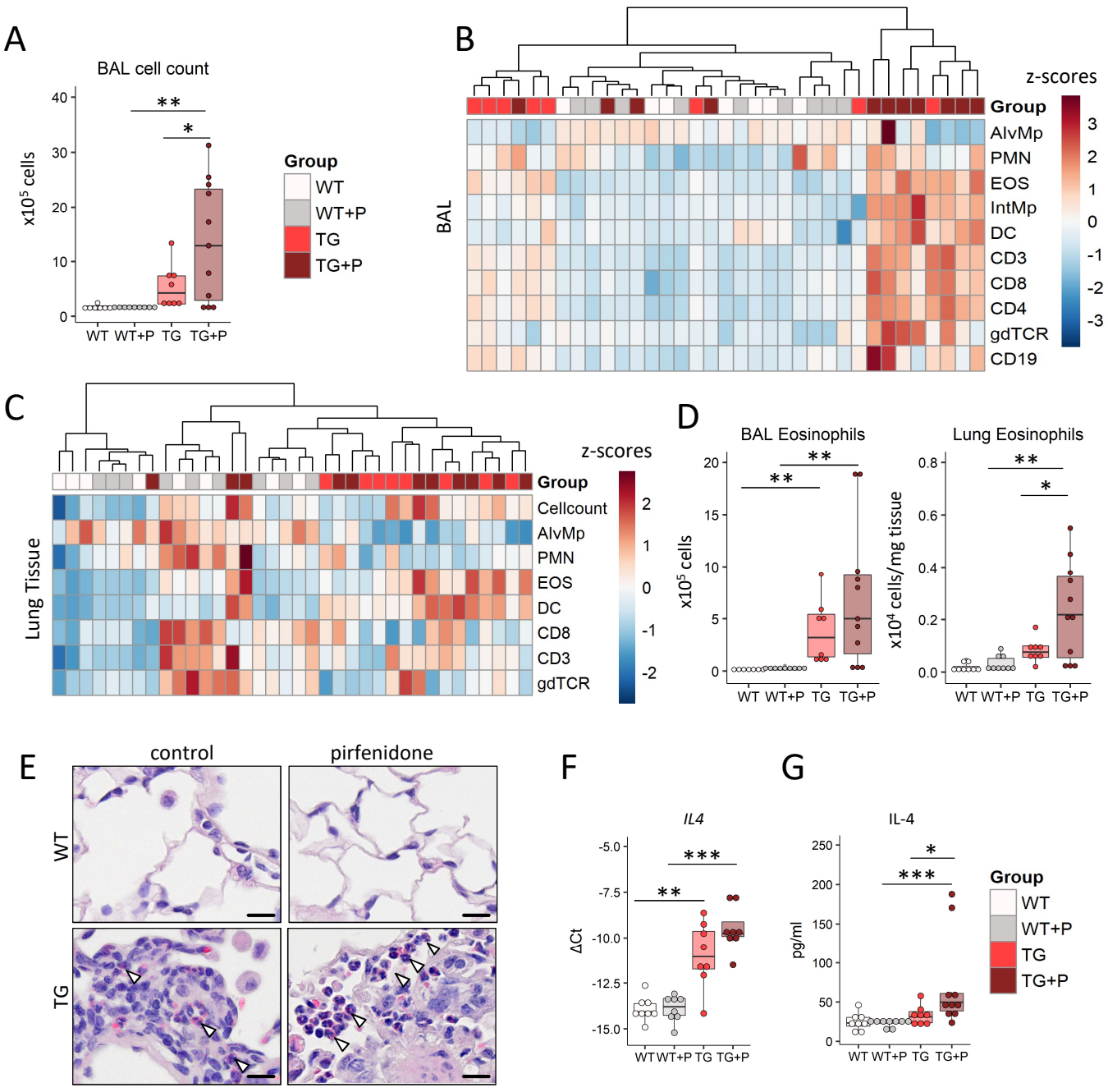
A
BAL cell count
x10^5 cells
40
30
20
10
0
**
*
WT WT+P TG TG+P
Group
WT
WT+P
TG
TG+P
B
z-scores
3
2
1
0
-1
-2
-3
BAL
Group
AlvMp
PMN
EOS
IntMp
DC
CD3
CD8
CD4
gdTCR
CD19
C
Lung Tissue
z-scores
2
1
0
-1
-2
Group
Cellcount
AlvMp
PMN
EOS
DC
CD8
CD3
gdTCR
D
BAL Eosinophils
x10^5 cells
20
15
10
5
0
**
**
WT WT+P TG TG+P
Lung Eosinophils
x10^4 cells/mg tissue
0.8
0.6
0.4
0.2
0.0
**
*
WT WT+P TG TG+P
E
control
pirfenidone
WT
TG
F
IL4
ΔCt
-5.0
-7.5
-10.0
-12.5
-15.0
***
**
WT WT+P TG TG+P
G
IL-4
pg/ml
250
200
150
100
50
0
*
***
WT WT+P TG TG+P
Group
WT
WT+P
TG
TG+P

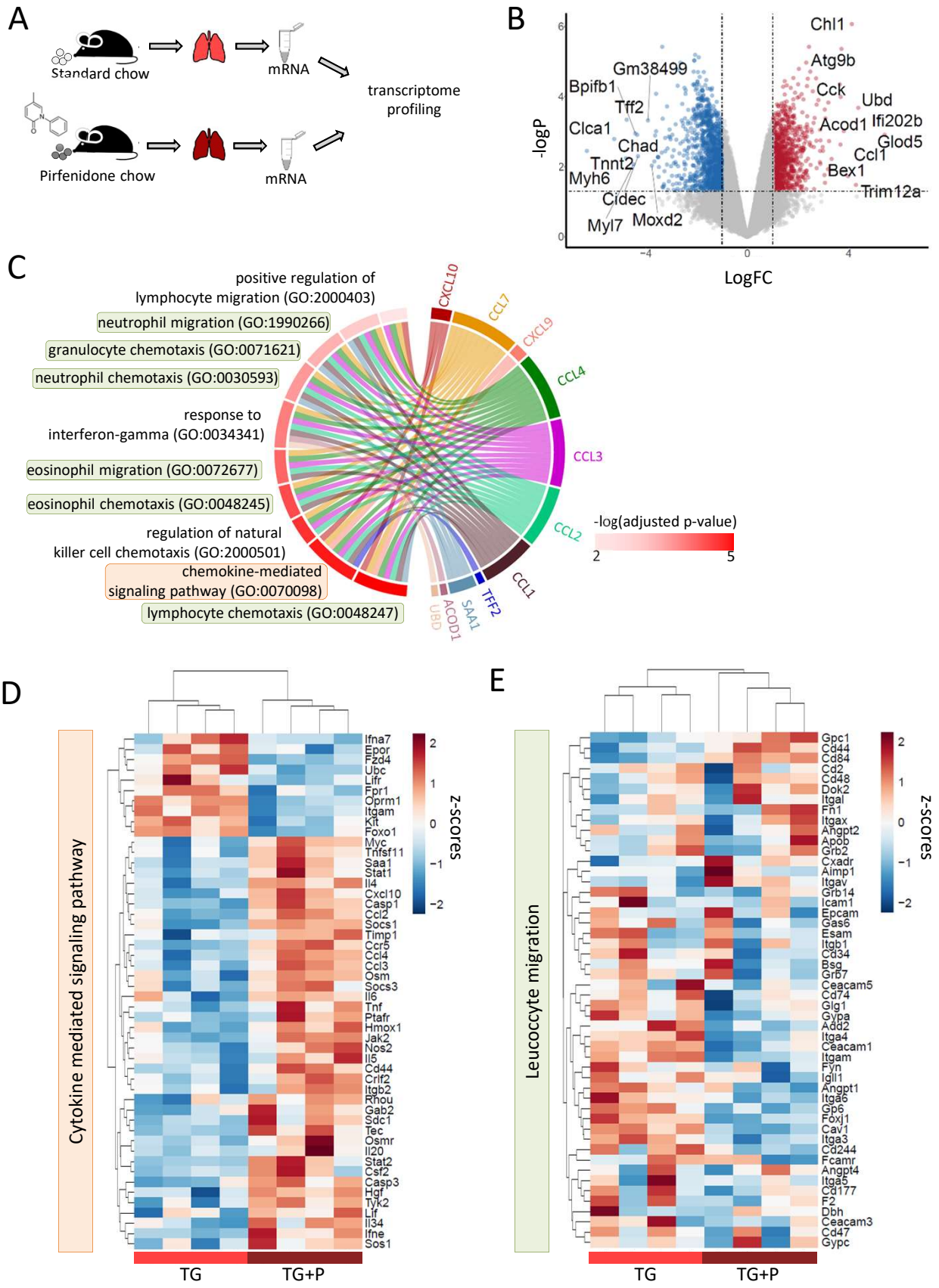
A
Standard chow
mRNA
transcriptome profiling
Pirfenidone chow
mRNA
B
-logP
LogFC
Chl1
Atg9b
Cck
Ubd
Ifi202b
Glod5
Ccl1
Bex1
Trim12a
Acod1
Gm38499
Bpifb1
Tff2
Clca1
Chad
Tnnt2
Myh6
Cidec
Myl7
Moxd2
C
positive regulation of lymphocyte migration (GO:2000403)
neutrophil migration (GO:1990266)
granulocyte chemotaxis (GO:0071621)
neutrophil chemotaxis (GO:0030593)
response to interferon-gamma (GO:0034341)
eosinophil migration (GO:0072677)
eosinophil chemotaxis (GO:0048245)
regulation of natural killer cell chemotaxis (GO:2000501)
chemokine-mediated signaling pathway (GO:0070098)
lymphocyte chemotaxis (GO:0048247)
CXCL10
CCL7
CXCL9
CCL4
CCL3
CCL2
CCL1
TFF2
SAA1
ACOD1
UBD
-log(adjusted p-value)
2
5
D
Cytokine mediated signaling pathway
z-scores
TG
TG+P
E
Leucocyte migration
z-scores
TG
TG+P

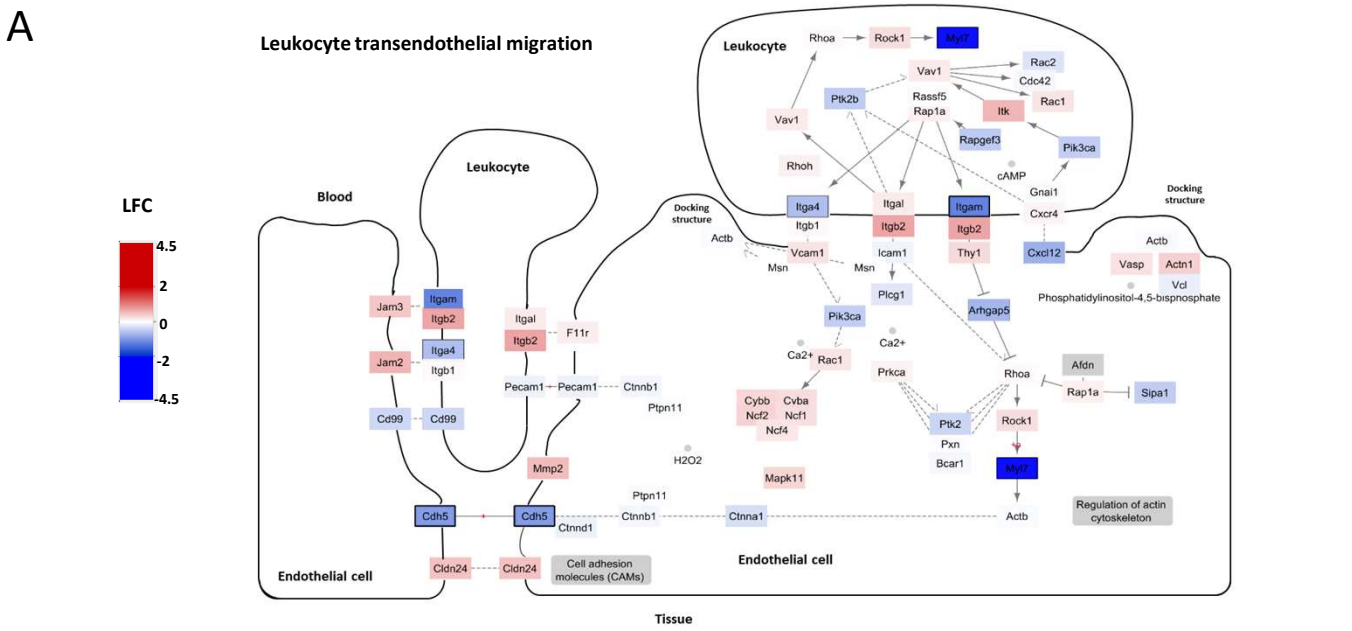
A
Leukocyte transendothelial migration
LFC
4.5
2
0
-2
-4.5
Blood
Leukocyte
Tissue
Endothelial cell
Endothelial cell
Docking structure
Cell adhesion molecules (CAMs)
Regulation of actin cytoskeleton
Phosphatidylinositol-4,5-bispnosphate
Rhoa
Rock1
Vav1
Rac2
Cdc42
Rac1
Ptk2b
Rassf5
Rap1a
Itk
Rapgef3
Pik3ca
Rhoh
cAMP
Gnai1
Cxcr4
Cxcl12
Itga4
Itgal
Itgam
Itgb1
Itgb2
Thy1
Vcam1
Icam1
Msn
Actb
Vasp
Actn1
Vcl
Plcg1
Pik3ca
Arhgap5
Ca2+
Rac1
Prkca
Rhoa
Afdn
Rap1a
Sipa1
Ptk2
Pxn
Bcar1
Rock1
Jam3
Jam2
Cd99
F11r
Pecam1
Ctnnb1
Ptpn11
Cybb
Cyba
Ncf2
Ncf1
Ncf4
H2O2
Mmp2
Mapk11
Cdh5
Ctnnd1
Ctnna1
Cldn24
B
Cdh5
ΔCt
WT
WT+P
TG
TG+P
C
WT
WT+P
TG
TG+P
inset
Cdh5
Vwf
DAPI
D
BAL cell count
R = −0.52
p = 0.0014
Cdh5

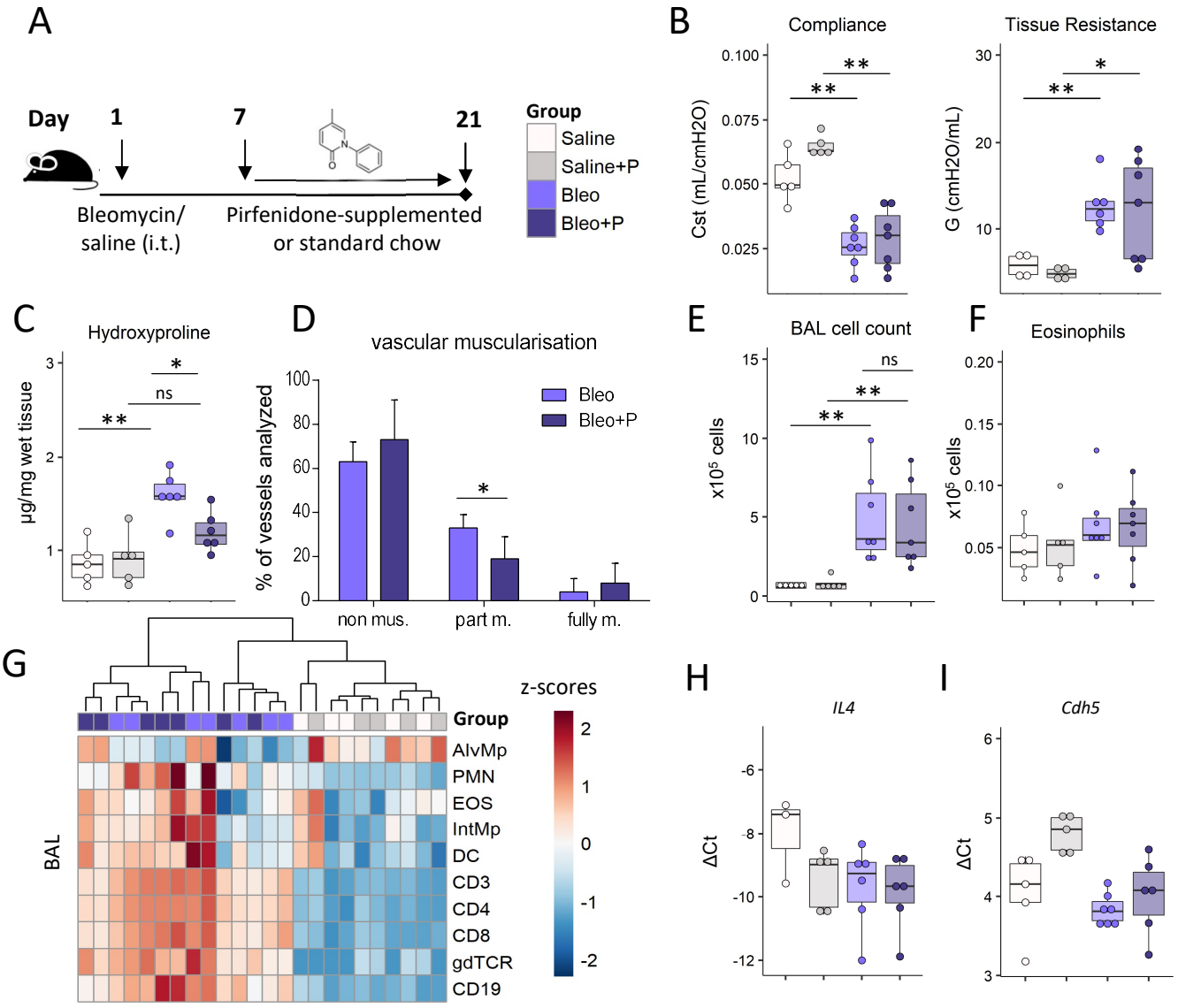
A
Day
1
7
21
Bleomycin/
saline (i.t.)
Pirfenidone-supplemented
or standard chow
Group
Saline
Saline+P
Bleo
Bleo+P
B
Compliance
Cst (mL/cmH2O)
Tissue Resistance
G (cmH2O/mL)
C
Hydroxyproline
µg/mg wet tissue
D
vascular muscularisation
% of vessels analyzed
non mus.
part m.
fully m.
E
BAL cell count
x10⁵ cells
F
Eosinophils
G
z-scores
BAL
AlvMp
PMN
EOS
IntMp
DC
CD3
CD4
CD8
gdTCR
CD19
H
IL4
ΔCt
I
Cdh5
ΔCt

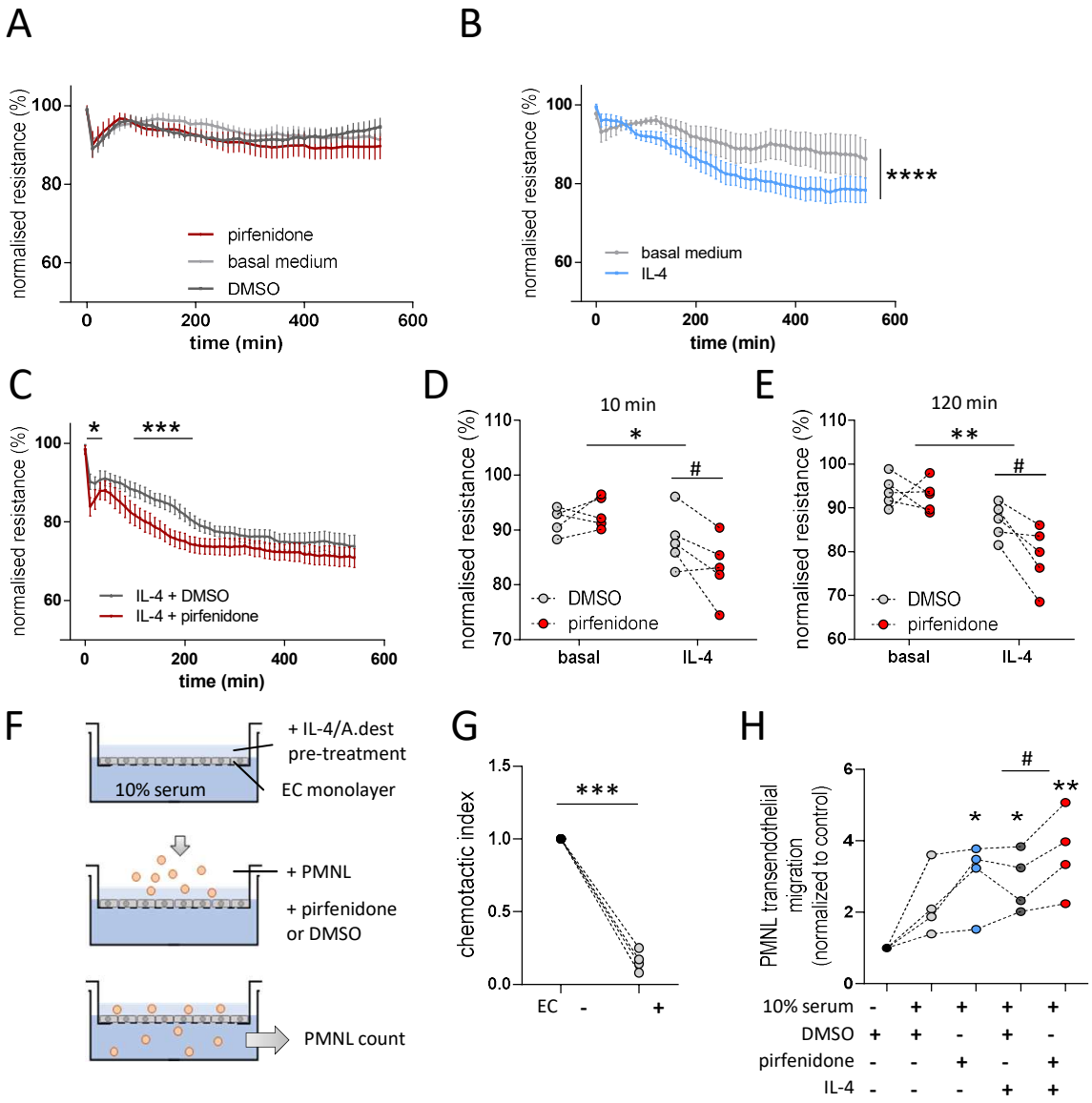
A
normalised resistance (%)
100
80
60
pirfenidone
basal medium
DMSO
0
200
400
600
time (min)
B
normalised resistance (%)
100
80
60
****
basal medium
IL-4
0
200
400
600
time (min)
C
normalised resistance (%)
100
80
60
*
***
IL-4 + DMSO
IL-4 + pirfenidone
0
200
400
600
time (min)
D
10 min
normalised resistance (%)
110
100
90
80
70
*
#
DMSO
pirfenidone
basal
IL-4
E
120 min
normalised resistance (%)
110
100
90
80
70
60
**
#
DMSO
pirfenidone
basal
IL-4
F
+ IL-4/A.dest
pre-treatment
10% serum
EC monolayer
+ PMNL
+ pirfenidone
or DMSO
PMNL count
G
chemotactic index
1.5
1.0
0.5
0.0
***
EC
-
+
H
PMNL transendothelial
migration
(normalized to control)
6
4
2
0
#
**
*
*
10% serum - + + + +
DMSO + + - + -
pirfenidone - - + - +
IL-4 - - - + +

Pirfenidone exacerbates Th2-driven vasculopathy in a mouse model of SSc-ILD

Birnhuber Anna[1,2], Jandl Katharina[1,3], Biasin Valentina[1,2], Fließer Elisabeth[1], Valzano Francesco[1], Marsh Leigh M[1], Krolczik Christina[4], Olschewski Andrea[1,5], Wilhelm Jochen[6], Toller Wolfgang[5], Heinemann Akos[3], Olschewski Horst[1,7], Wygrecka Malgorzata[4], Kwapiszewska Grazyna[1,2,8].

[1] Ludwig Boltzmann Institute for Lung Vascular Research Graz, Austria.

[2] Otto Loewi Research Center, Division of Physiology, Medical University of Graz, Graz, Austria.

[3] Otto Loewi Research Center, Division of Pharmacology, Medical University of Graz, Graz, Austria.

[4] Center for Infection and Genomics of the Lung, Universities of Giessen and Marburg Lung Center, Giessen, Germany. Member of the German Center for Lung Research.

[5] Department of Anaesthesiology and Intensive Care Medicina, Medical University of Graz, Graz, Austria.

[6] Department of Internal Medicine, Universities of Giessen and Marburg Lung Center, Giessen, Germany.

[7] Division of Pulmonology, Department of Internal Medicine, Medical University of Graz, Graz, Austria.

[8] Institute for Lung Health (ILH), Justus Liebig University, Giessen, Germany

*Corresponding author:

Grazyna Kwapiszewska

Ludwig Boltzmann Institute for Lung Vascular Research

Neue Stiftingtalstrasse 6/VI

8010 Graz, Austria

Phone number: +43 316 385-72918

E-mail: Grazyna.Kwapiszewska@lvr.lbg.ac.at

SUPPLEMENTAL MATERIALS

MATERIAL AND METHODS

Animal experiments

Female Fra-2 overexpressing/transgenic (Fra-2 TG) mice and wild-type (WT) littermates were maintained under specific pathogen free conditions in isolated ventilated cages with 12-hour light/dark cycles. All animal experiments met EU guidelines 2010/63/EU and were approved by the local authorities (Austrian Ministry of Education, Science and Culture). Bleomycin was given intra-tracheally at a dose of 0.8 units per kg bodyweight as described previously [1, 2]. Pirfenidone treatment protocol was adapted from previous publications [3] and incorporated into standard laboratory chow at 2.8 mg/g (Sniff, Soest, Germany). Pirfenidone was provided by HOFFMANN-LA ROCHE. Food was weighed regularly and mean pirfenidone uptake was calculated. Mean pirfenidone uptake was approximately 400 mg/kg bodyweight per day, a frequently used dosage in mouse studies, leading to pirfenidone exposure ratios and plasma concentrations similar to those in patients treated with pirfenidone [4–6]. Pirfenidone treatment of Fra-2 TG and WT mice was performed in two independent experiments with five to eight mice per group. Schematic representations of Fra-2 TG and bleomycin experiments are shown in Figures 1A and 5A, respectively. Treatment of Fra-2 TG and WT mice with the glucocorticoid budesonide was described and published previously [7].

Lung function measurements

Following pirfenidone treatment, lung function of Fra-2 TG and WT littermate control mice with and without pirfenidone treatment was measured. To this end, mice were anesthetized using a combination of 150 mg/kg ketamine and 20 mg/kg xylazine, intubated and mechanically ventilated (frequency: 150 breaths/min, tidal volume: 10 ml/kg and positive end expiratory pressure: 2 cmH2O). Lung function was measured using a flexiVent FX1 module (SciReq, Canada).

Bronchoalveolar lavage fluid (BALF)

Following lung function measurements, mice were sacrificed by exsanguination and lungs were lavaged with 1 ml PBS containing protease inhibitor cocktail (Roche) and 1 mM EDTA. BALF was centrifuged and total cell counts were made, the supernatant was frozen and stored at -80°C until further analysis.

Single cell lung tissue homogenates

Single cell suspensions from lung tissue were performed as previously described [3]. In short, the lower right lobe was digested in medium containing 0.7 mg/ml collagenase and 30 µg/ml DNAse for 40 min at 37°C. Tissue was passed through a 100 µm cell strainer to obtain a single cell suspension. Erythrocytes were lysed for 5 min using ammonium chloride buffer.

Inflammatory cell profiling (Flow cytometry)

BAL cells and single cell lung tissue homogenates were analysed using a LSRII flow cytometer and analysed with the FACSDiva software (BD Biosciences) as previously described [4]. Cells were initially gated on CD45 positivity and were identified as follows: neutrophils (CD11b+, CD11c-, Gr-1+), macrophages (CD11b low, CD11c+, Siglec-F+), dendritic cells (CD11b+, CD11c+, MHC-II high), T helper cells (CD3+, CD4+), cytotoxic T cells (CD3+, CD8+), B cells (CD19+), and eosinophils (CD11b+, CD11c-, Siglec F+). Antibody details are provided in Table 1. For the heatmap presentation, data was normalised using sqrt(sqrt(cellcount)). z-scores cell counts are shown.

Immunofluorescence and tissue staining

Lung tissue samples were formalin-fixed, paraffin embedded and cut into 2.5 µm sections. Sections were deparaffinised and rehydrated in decreasing concentrations of ethanol. Tissue sections were stained with Masson's trichrome or Sirius red for histological collagen analysis. Eosinophils were stained using 1% Chromotrop 2R (St. Louis, MO, US) in aqueous solution for 10 min, followed by hemalaun nuclear counterstain. To quantify the degree of muscularisation, lung tissue sections were stained by double immunohistochemistry with the

endothelial cell marker von Willebrand factor (vWF) and α-smooth muscle actin (α-Sma) as described previously [5].

Immunofluorescence staining was performed on rehydrated tissue sections with antigen retrieval performed in sodium citrate pH6 buffer. Blocking was performed using 5% donkey serum. Sections were incubated with primary antibodies against VE-Cadherin (1:50, R&D Systems) and von Willebrand factor (1:500, Dako) overnight at 4°C, followed by washing and incubation with Alexa Fluor-488/647-labelled secondary antibodies (Life Technologies) at room temperature for 30 min. Negative controls were performed alongside by omission of the first antibody. Slides were mounted with Vectashield DAPI containing mounting medium (Vector Laboratories, Burlingame, CA).

Chamber slides were blocked with 0.1% Triton X and 3% BSA in PBS for one h at room temperature. Unconjugated primary antibodies were diluted in the same buffer and slides were incubated overnight at 4°C. The following day, slides were incubated with Alexa Fluor-488/647-labelled secondary antibodies and AF555 pre-labelled anti-Phalloidin antibody. Slides were mounted with Vectashield DAPI containing mounting medium (Vector Laboratories). All images were taken using a laser scanning confocal microscope (Nikon A1R Ultra-Fast Spectral Scanning Confocal Microscope) with a CFI Plan Apochromat Lambda 60x/1.4 oil immersion objective.

Quantification of vascular remodelling and histological scoring

Tissue sections were analysed using Visiopharm integrated software VIS (Visiopharm, Denmark). Per mouse, 150±67 (minimum: 34, maximum 234) vessels, ranging from 10 to 100 µm in size, were analysed. Deposition of collagen was analysed on Sirius red stained sections, as described previously [5]. To acquire values indicative of parenchymal collagen deposition, bronchi and vessels with a diameter larger than 200 µm were excluded from analysis.

Hydroxyproline measurements

Lung tissue was weighed and hydrolized in 2 N NaOH for eight hours at 120°C. Hydroxyproline measurements were performed as previously published [10].

Western blotting

Proteins from mouse lung homogenate samples were isolated using RIPA buffer (Sigma). Protein samples were separated by SDS-PAGE and transferred to PVDF membranes (GE Healthcare, UK). Membranes were incubated with primary antibodies (Collagen 1, 1:1000; Southern Biotech, USA, and α-tubulin, 1:1000; Cell Signaling Technologies, USA) at 4°C overnight, followed by one h incubation at room temperature with HRP-conjugated secondary antibodies. Membranes were incubated with ECL prime developing solution (GE Healthcare, UK). Signal detection was done using a ChemiDoc Touch Imaging System (Bio-Rad, USA).

RNA isolation and real-time RT-PCR

Total RNA was isolated from lung homogenates using the peqGOLD Total RNA Kit (Peqlab, Germany) and reverse transcribed using the iScript cDNA Synthesis kit (Bio-Rad, USA). The real-time RT-PCR reaction was run on a LightCycler 480 System (Roche Applied Science, Austria) using the QuantiFast SYBR Green PCR kit (Qiagen, Germany). Hydroxymethylbilane synthase (HMBS) and beta-2-microglobulin (B2M) were used as reference genes. The threshold cycle (Ct) difference was calculated as follows: ΔCt = mean Ct reference genes – Ct target gene.

Transcriptomic profiling

Total RNA was isolated from lungs using the RNeasy Mini kit (Peqlab, Erlangen, Germany). 200 ng of total RNA was pre-amplified and labelled with Cy5 using the Low-input QuickAmp Kit (Agilent Technology, Santa Clara, CA) according to the manufacturer's instructions. Hybridizations were performed for 18 h at 42°C on Agilent 6x80K mouse microarrays in Agilent hybridization chambers. Data were analysed using the limma package in R. Intensity values were background-corrected and quantile normalized. Significance of differential expression was estimated using moderated t-statistics as previously described in full [6].

Data visualization was performed in R programming environment using Rstudio (version 1.3.952). Volcano plots were computed using “EnhancedVolcano” Bioconductor package version 1.6.0. Variable genes across the two experimental groups were identified imposing a significance threshold (-log adjusted p-value) of 1.3 and FC of 1. Colour coding was assigned according to higher enrichment in wild-type animals or transgenic animals. Heatmaps were computed using “pheatmap” package version 1.0.12. Hierarchical clustering was performed to address similarities in each experimental animal in the two groups, respectively. Differential gene expression is shown in single animals and colour coded according “RdYlBl” color palette. Gene Ontology analysis was performed using enrichr [7–9] using the Gene Ontology Biological Process 2018 reference database. P-value adjustment was performed with Benjamini-Hochberg multiple test correction method. Top 10 GO enrichment terms were identified by filtering out terms with adjusted p-value >0.05 and colour coded according to significance power (-log adjusted p-value > 1.3). Chord diagram was computed using “chorddiag” package version 0.1.3 using as input gene ontology results.

Isolation of eosinophils

Blood for the isolation of human eosinophils was collected from healthy volunteers according to a protocol approved by the Ethics Committee of the Medical University of Graz (17-291 ex 05/06), as previously described [10]. In brief, citrated blood was centrifuged at 400 x g, for 20 min to remove plasma. Erythrocytes were eliminated via dextran sedimentation. Peripheral blood mononuclear cells (PBMCs) and polymorphonuclear leukocytes (PMNL) were separated via density gradient centrifugation on Histopaque 1.077 layer. Eosinophil isolation was done from the PMNL fraction by negative selection using the MACS cell separation system, containing a cocktail of biotin-conjugated monoclonal antibodies against CD2, CD14, CD16, CD19, CD56, CD123, and CD235a (Glycophorin A) (Eosinophil Isolation Kit, Miltenyi Biotec, Bergisch Gladbach, Germany), according to manufacturer’s protocol. Purity typically yielded >98 %.

Eosinophil shape change

Eosinophil shape change was measured as previously described [10]. In short, purified eosinophils were kept in assay buffer containing Ca^{2+} and Mg^{2+} ($1x10^6$/mL). Cells were equally divided into reaction tubes and serial dilutions of pirfenidone or eotaxin-2 (diluted in assay buffer) were added. Cells were incubated in the water bath for 4 min at 37°C followed by immediate transfer to ice and addition of 150 µl of fixative solution on ice, to stop the reaction. Cells were analysed on a FACSCaliburTM (BD Biosciences, NJ, US) and eosinophil shape change was detected as an increase of the forward scatter and was normalized to the respective vehicle control.

Eosinophil chemotaxis

Eosinophil chemotaxis was assessed as previously described [10]. Isolated human eosinophils were resuspended in assay buffer with Ca^{2+} and Mg^{2+} ($1x10^6$/mL), with or without pirfenidone pre-treatment, and placed into top wells of a micro-Boyden chamber with 3 µm pores (NeuroProbe Inc, Gaithersburg, MD, USA) and incubated at 37°C. Eosinophils were allowed to migrate towards increasing concentrations of eotaxin-2 (CCL24, Immunotools, Friesoythe, Germany) for one h. Migrated cells in the bottom wells of the chambers were counted by flow cytometry.

Eosinophil reactive oxygen species production

Production of reactive oxygen species (ROS) was measured as previously described [10]. Isolated human eosinophils were resuspended in assay buffer with Ca^{2+} and Mg^{2+} ($1x10^6$/mL) containing 5 µM dihydrorhodamine 123 and 100 µM pirfenidone, for 30 min at 37°C. Recombinant C5a peptide served as positive control. To stop the reaction samples were transferred to ice, fixed and analyzed by flow cytometry. ROS production was detected as an increase of fluorescence in the FL-1 channel due to the oxidization of the non-fluorescent dye dihydrorhodamine 123 into fluorescent rhodamine 123. Data are shown as fold change to vehicle control.

Lung microvascular endothelial cell culture

Human lung microvascular endothelial cells (HMVEC) purchased from LONZA were cultured in EGM^{TM}-2 endothelial cell media supplemented with microvascular endothelial cell supplementary kit C-22121 (Lonza, Basel, Switzerland) T75 flasks coated with 1% gelatine as previously reported [11]. HMVEC were cultured on 8-well chamber slides. When reaching confluence, medium was changed to EBM^{TM}-2 basal medium supplemented with 2.5% fetal bovine serum and 1% Penicillin/Streptomycin overnight. Next day, cells were pre-treated with IL-4 (20 ng/ml, Immunotools, Friesoythe, Germany), followed by treatment with 500 µM pirfenidone dissolved in DMSO. DMSO alone served as negative control. After 15 min, cells were washed, fixed with 4% PFA in PBS Plus buffer supplemented with 1% BSA and stored at 4°C until further use.

Electrical cell-substrate impedance sensing

Human lung microvascular endothelial cells (LONZA, Basel, CH) were cultured in EGM^{TM}-2 endothelial cell growth medium (LONZA, Basel, Switzerland) on 8W10E+ PET Chips pre-activated with 10 mM L-cystein (AppliedBiophysics, NY, USA) until reaching confluence as previously reported [11, 12]. Medium was changed to EBM^{TM}-2 basal medium supplemented with 2.5% fetal bovine serum and 1% penicillin/streptomycin overnight. Endothelial barrier integrity was monitored by electrical cell-substrate impedance sensing (ECIS® Z-Theta, AppliedBiophysics, NY, USA) upon stimulation with IL-4 (20 ng/ml) and pirfenidone 500 µM dissolved in DMSO. The same concentrations of DMSO were used as vehicle control.

Transmigration assay

HMVEC were seeded on 96-well Transwell inserts pre-coated with 1% gelatin (3 µm pore size, polycarbonate membrane) (Corning, Lactan, Austria) at a density of 20.000 cells/well in EGM-2 MV growth medium. The following day, HMVECs were pre-treated with vehicle or IL-4 (20 ng/mL) for two h in basal RPMI media (Thermo Fischer, U.S.A). After two h, HMVEC were treated with pirfenidone or vehicle together with the addition of 0.1 x 10^6 polymorphnuclear cells (PMNL) per well to the upper compartment. PMNL were allowed to

migrate to the lower compartment supplied with RPMI with 10% FBS or 0% FBS, respectively, for 2.5 h in humidified incubator at 37°C. Subsequently, PMNL were collected from lower compartment and fixed with 100 µl of fixative solution on ice. Migrated cells were counted by flow cytometry FACSCaliburTM (BD Biosciences, NJ, US).

References

1. Biasin V, Crnkovic S, Sahu-Osen A, Birnhuber A, el Agha E, Sinn K, Klepetko W, Olschewski A, Bellusci S, Marsh LM, Kwapiszewska G. PDGFRα and αSMA mark two distinct mesenchymal cell populations involved in parenchymal and vascular remodeling in pulmonary fibrosis. *American Journal of Physiology-Lung Cellular and Molecular Physiology* 2020; 318: L684–L697.

2. Bordag N, Biasin V, Schnoegl D, Valzano F, Jandl K, Nagy BM, Sharma N, Wygrecka M, Kwapiszewska G, Marsh LM. Machine Learning Analysis of the Bleomycin Mouse Model Reveals the Compartmental and Temporal Inflammatory Pulmonary Fingerprint. *iScience* 2020; 23: 101819.

3. Kehrer JP, Margolin SB. Pirfenidone diminishes cyclophosphamide-induced lung fibrosis in mice. *Toxicology Letters* 1997; 90.

4. Schaefer CJ, Ruhrmund DW, Pan L, Seiwert SD, Kossen K. Antifibrotic activities of pirfenidone in animal models. *European Respiratory Review* 2011; 20.

5. Kakugawa T, Mukae H, Hayashi T, Ishii H, Abe K, Fujii T, Oku H, Miyazaki M, Kadota J, Kohno S. Pirfenidone attenuates expression of HSP47 in murine bleomycin-induced pulmonary fibrosis. *European Respiratory Journal* 2004; 24: 57–65.

6. Kehrer JP, Margolin SB. Pirfenidone diminishes cyclophosphamide-induced lung fibrosis in mice. *Toxicology Letters* 1997; 90: 125–132.

7. Gungl A, Biasin V, Wilhelm J, Olschewski A, Kwapiszewska G, Marsh LM. Fra2 Overexpression in Mice Leads to Non-allergic Asthma Development in an IL-13 Dependent Manner. *Frontiers in Immunology* 2018; 9.

8. Nagaraj C, Haitchi HM, Heinemann A, Howarth PH, Olschewski A, Marsh LM. Increased Expression of p22phox Mediates Airway Hyperresponsiveness in an Experimental Model of Asthma. *Antioxidants & Redox Signaling* 2017; 27.

9. Birnhuber A, Crnkovic S, Biasin V, Marsh LM, Odler B, Sahu-Osen A, Stacher-Priehse E, Brcic L, Schneider F, Cikes N, Ghanim B, Klepetko W, Graninger W, Allanore Y, Eferl R, Olschewski A, Olschewski H, Kwapiszewska G. IL-1 receptor blockade skews inflammation towards Th2 in a mouse model of systemic sclerosis. *European Respiratory Journal* 2019; 54.

10. Kesava Reddy G, Enwemeka CS. A simplified method for the analysis of hydroxyproline in biological tissues. *Clinical Biochemistry* 1996; 29: 225–229.

11. Hoffmann J, Wilhelm J, Marsh LM, Ghanim B, Klepetko W, Kovacs G, Olschewski H, Olschewski A, Kwapiszewska G. Distinct Differences in Gene Expression Patterns in Pulmonary Arteries of Patients with Chronic Obstructive Pulmonary Disease and Idiopathic Pulmonary Fibrosis with Pulmonary Hypertension. *American Journal of Respiratory and Critical Care Medicine* 2014; 190.

12. Xie Z, Bailey A, Kuleshov M v., Clarke DJB, Evangelista JE, Jenkins SL, Lachmann A, Wojciechowicz ML, Kropiwnicki E, Jagodnik KM, Jeon M, Ma'ayan A. Gene Set Knowledge Discovery with Enrichr. *Current Protocols* 2021; 1.

13. Kuleshov M v., Jones MR, Rouillard AD, Fernandez NF, Duan Q, Wang Z, Koplev S, Jenkins SL, Jagodnik KM, Lachmann A, McDermott MG, Monteiro CD, Gundersen GW, Ma'ayan A. Enrichr: a comprehensive gene set enrichment analysis web server 2016 update. *Nucleic Acids Research* 2016; 44.

14. Chen EY, Tan CM, Kou Y, Duan Q, Wang Z, Meirelles G, Clark NR, Ma'ayan A. Enrichr: interactive and collaborative HTML5 gene list enrichment analysis tool. *BMC Bioinformatics* 2013; 14.

15. Theiler A, Bärnthaler T, Platzer W, Richtig G, Peinhaupt M, Rittchen S, Kargl J, Ulven T, Marsh LM, Marsche G, Schuligoi R, Sturm EM, Heinemann A. Butyrate ameliorates allergic airway inflammation by limiting eosinophil trafficking and survival. *Journal of Allergy and Clinical Immunology* 2019; 144.

16. Rittchen S, Rohrer K, Platzer W, Knuplez E, Bärnthaler T, Marsh LM, Atallah R, Sinn K, Klepetko W, Sharma N, Nagaraj C, Heinemann A. Prostaglandin D2 strengthens human endothelial barrier by activation of E-type receptor 4. *Biochemical Pharmacology* 2020; 182.

17. Jandl K, Marsh LM, Hoffmann J, Mutgan AC, Baum O, Bloch W, Thekkekara-Puthenparampil H, Kolb D, Sinn K, Klepetko W, Heinemann A, Olschewski A, Olschewski H, Kwapiszewska G. Basement Membrane Remodeling Controls Endothelial Function in Idiopathic Pulmonary Arterial Hypertension. *American Journal of Respiratory Cell and Molecular Biology* 2020; 63.

Tables

Table1: Details for antibodies used for flow cytometry analysis of inflammatory cell populations in bronchoalveolar lavage and lung tissue of mice.

Antigen	Label	Panel	Company	Clone	Isotype	Dilution Factor
CD19	BB515	1	BD Bioscience	1D3	Rat IgG2a, κ	1:50
CD4	APC	1	Biolegend	GK1.5	Rat IgG2b, κ	1:100
CD8	PE	1	Biolegend	53-6.7	Rat IgG2a, κ	1:200
CD11b	BV510	2	BD Bioscience	M1/70	Rat IgG2b, κ	1:50
CD11c	ef450	2	eBioscience	N418	Armenian Hamster IgG	1:50
CD3	AF700	1	Biolegend	500A2	Syrian Hamster IgG	1:50
CD24	PerCP Cy5.5	2	BD Bioscience	M1/69	Rat IgG2b, κ	1:500
CD25	APC-Cy7	1	Biolegend	PC61	Rat IgG1, λ	1:50
CD45	PerCP-Cy5.5	1	eBioscience	30-F11	Rat IgG2b, κ	1:200
CD45	AF488	2	eBioscience	30-F11	Rat IgG2b, κ	1:200
CD64	AF647	2	BD Bioscience	X54-5/7.1	Mouse IgG1, κ	1:20
gdTCR	BV421	1	Biolegend	GL3	Hamster IgG	1:50
Gr-1	PE-Cy7	2	Biolegend	RB6-8C5	Rat IgG2b, κ	1:800
MHC-II	APC-Cy7	2	Biolegend	M5/114.15.2	Rat IgG2b, κ	1:400
Siglec F	PE	2	BD Bioscience	E50-2440	Rat IgG2a, κ	1:20

Figure Legends

Figure S1: Masson's trichrome stainings of the left lung lobes of WT and TG mice with (+P) and without pirfenidone treatment. Four representative lungs per groups are shown. Scalebar = 1 mm

Figure S2: Budesonide ameliorates parenchymal collagen deposition in Fra-2 TG mice. Quantification of sirius red collagen staining on lung sections from WT and TG mice with (+Bude) and without treatment with the glucocorticosteroid budesonide. Left graph depicts % of collagen within the tissue. Right graph depicts tissue density (% of tissue compared to the whole area analysed).

Figure S3: Pirfenidone does not exert any direct effect on eosinophil activation, chemotaxis or survival. (A) Shape change measurement of eosinophils in response to pirfenidone or eotaxin-2 with and without pirfenidone pre-treatment. Data are normalised to the corresponding vehicle control. FSC: forward scatter. (B) Chemotaxis measurement (micro Boyden chamber) in response to eotaxin-2 with ant without pirfenidone pre-treatment. (C) Eosinophil ROS production measured by dihydrorhodamine 123 oxidation in response to C5a (positive control) or pirfenidone. Data are shown as fold change to the corresponding vehicle control. (D) Eosinophil survival after 3, 18 or 24 h in medium containing interleukin-5 (IL-5) and/or pirfenidone.

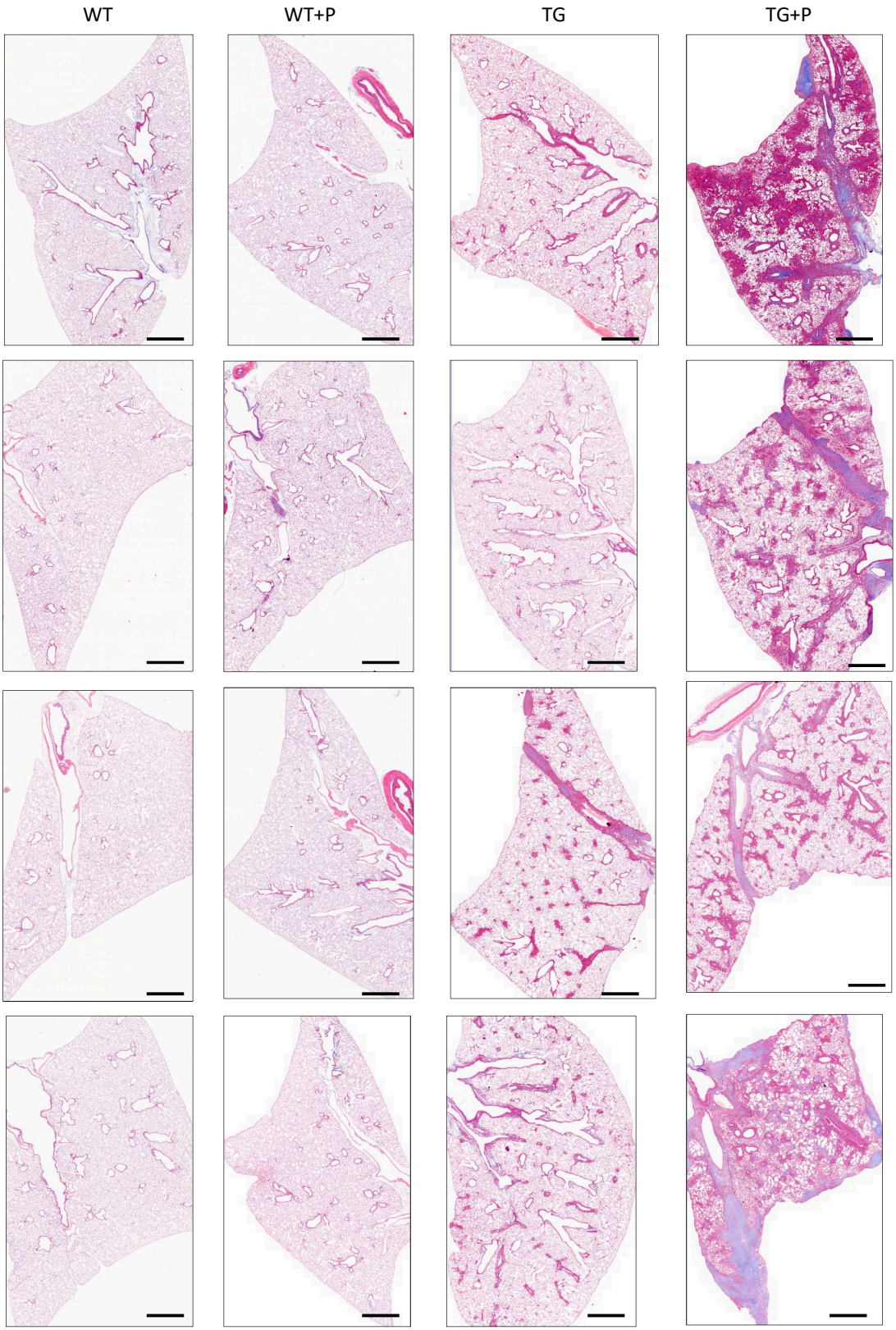
WT
WT+P
TG
TG+P

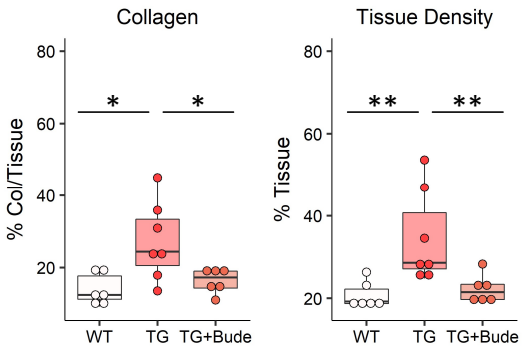
Collagen
% Col/Tissue
80
60
40
20
*
*
WT
TG
TG+Bude
Tissue Density
% Tissue
80
60
40
20
**
**
WT
TG
TG+Bude

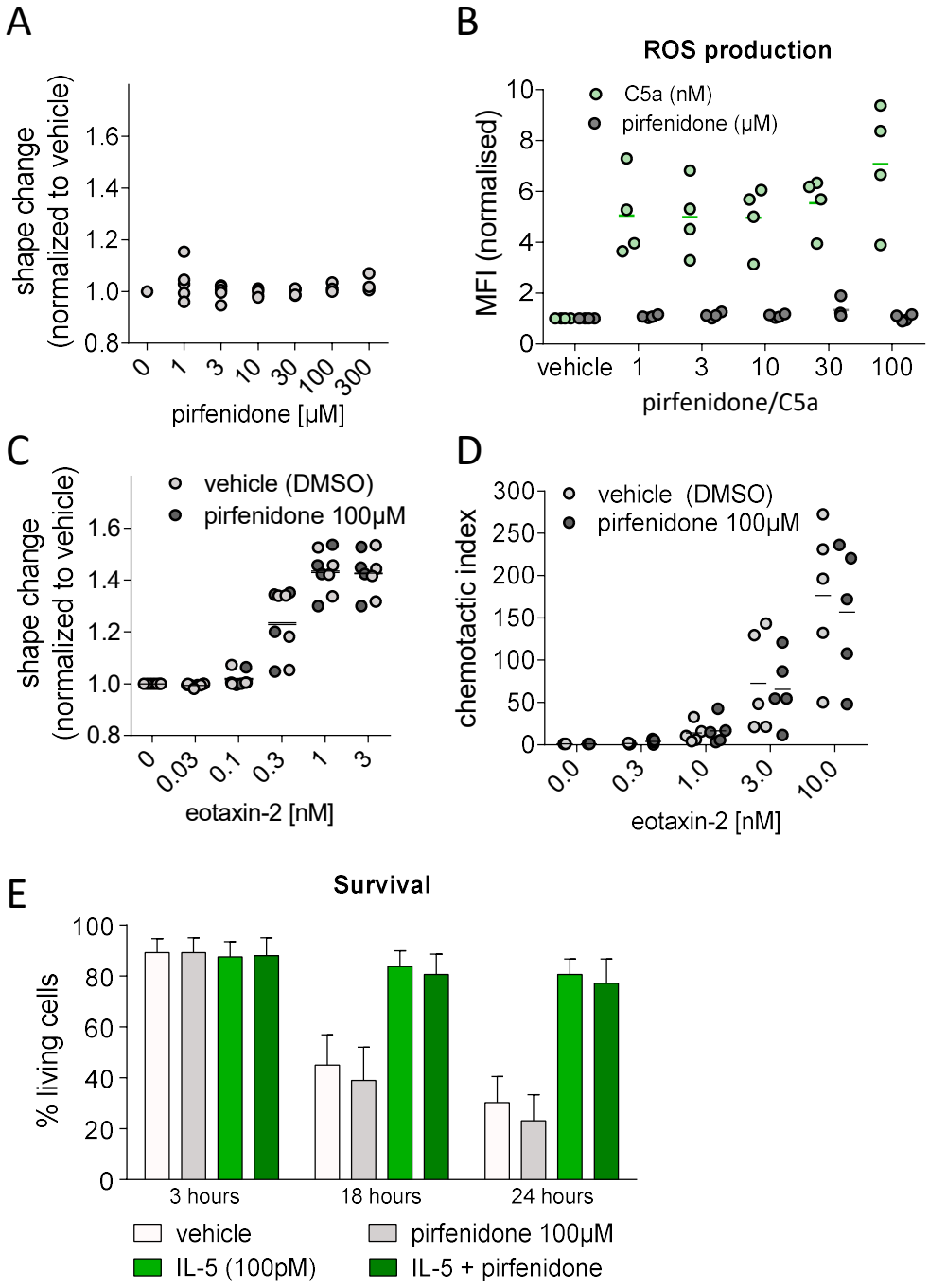
A
shape change (normalized to vehicle)
1.6
1.4
1.2
1.0
0.8
0
1
3
10
30
100
300
pirfenidone [µM]
B
ROS production
C5a (nM)
pirfenidone (µM)
MFI (normalised)
10
8
6
4
2
0
vehicle
1
3
10
30
100
pirfenidone/C5a
C
vehicle (DMSO)
pirfenidone 100µM
shape change (normalized to vehicle)
1.6
1.4
1.2
1.0
0.8
0
0.03
0.1
0.3
1
3
eotaxin-2 [nM]
D
vehicle (DMSO)
pirfenidone 100µM
chemotactic index
300
250
200
150
100
50
0
0.0
0.3
1.0
3.0
10.0
eotaxin-2 [nM]
E
Survival
% living cells
100
80
60
40
20
0
3 hours
18 hours
24 hours
vehicle
pirfenidone 100µM
IL-5 (100pM)
IL-5 + pirfenidone